African Smoke Particles Act as Cloud Condensation Nuclei in the Wintertime Tropical North Atlantic Boundary Layer over Barbados

Haley M. Royer[1], Mira L. Pöhlker[2,3,4*], Ovid Krüger[2], Edmund Blades[5,6], Peter Sealy[5], Nurun Nahar Lata[7], Zezhen Cheng[7], Swarup China[7], Andrew P. Ault[8], Patricia K. Quinn[9], Paquita Zuidema[1], Christopher Pöhlker[2], Ulrich Pöschl[2], Meinrat Andreae[2,10,11] and Cassandra J. Gaston[1*]

[1]Department of Atmospheric Sciences, Rosenstiel School of Marine~~, and~~ Atmospheric, and Earth Science, University of Miami, Miami, FL

[2]Department of Multiphase Chemistry, Max Planck Institute for Chemistry, Mainz, Germany

[3]Leipzig Institute for Meteorology, Leipzig University, Leipzig, Germany

[4]Experimental Aerosol and Cloud Microphysics Department, Leibniz Institute for Tropospheric Research, Leipzig, Germany

[5]Barbados Atmospheric Chemistry Observatory, Ragged Point, Barbados

[6]Queen Elizabeth Hospital Barbados, Bridgetown, Barbados

[7]Environmental Molecular Sciences Laboratory, Pacific Northwest National Laboratory, Richland, WA

[8]Department of Chemistry, University of Michigan, Ann Arbor, MI

[9]Pacific Marine Environmental Laboratory, National Oceanic and Atmospheric Administration, Seattle, WA

[10]Department of Geology and Geophysics, King Saud University, Riyadh, Saudi Arabia

[11]Scripps Institution of Oceanography, University of California San Diego, La Jolla, California, USA

*Corresponding Authors:

Mira L. Pöhlker: Email: poehlker@tropos.de, Phone: +49 6131 305 7020

Cassandra J. Gaston: Email: cgaston@rsmas.miami.edu, Phone: (305)-421-4979

Formatted: Not Strikethrough

Abstract

The number concentration and properties of aerosol particles serving as cloud condensation nuclei (CCN) are important for understanding cloud properties~~formation~~, including~~particularly~~ in the tropical Atlantic marine boundary layer (MBL) where marine cumulus clouds reflect incoming solar radiation and obscure the low-albedo ocean surface. Studies linking aerosol source, composition, and water uptake properties in this region have been conducted primarily during the summertime dust transport season, despite the region receiving a variety of aerosol particle types throughout the year. In this study, we compare size-resolved aerosol chemical composition data to the hygroscopicity parameter κ derived from size-resolved CCN measurements made during the EUREC^{4}A and ATOMIC campaigns from January to February 2020. We observed unexpected periods of wintertime long-range transport of African smoke and dust to Barbados. During these periods, the accumulation mode aerosol particle and CCN number concentrations as well as the proportions of dust and smoke particles increased, whereas ~~while~~ the average κ slightly decreased (κ = 0.46~~5~~±0.10) from marine background conditions (κ = 0.52±0.09~~8~~) when the particles were mostly composed of marine organics and sulfate. Size-resolved chemical analysis shows that smoke particles were the major contributor to the accumulation mode ~~aerosol~~ during long-range transport events, indicating that smoke is mainly responsible for the observed increase in CCN number concentrations. Earlier studies conducted at Barbados have mostly focused on the role of dust on CCN, but our results show that aerosol hygroscopicity and CCN number concentrations during wintertime long-range transport events over the tropical North Atlantic are also affected by African smoke~~ more than dust~~. Our findings highlight the importance of African smoke for atmospheric processes and cloud formation over the Caribbean.

Introduction

Aerosol particle number, size, hygroscopicity, and chemical mixing state determine cloud droplet formation and, thus, fundamentally affect the radiative properties and lifetime of clouds (Albrecht, 1989; McFiggans et al., 2006; Quinn et al., 2008; Twomey, 1977; Zuidema et al., 2008). Quantifying the effect of aerosols on cloud radiative forcing, however, is still the single largest source of uncertainty in predicting temperature increases associated with climate change (Forster et al., 2021). This uncertainty is especially important to resolve in marine regions where aerosol-cloud interactions are understudied, even though the majority of Earth's surface is covered by oceans (Carslaw et al., 2013). The existing literature that explores marine aerosol-cloud interactions does so primarily in the mid to high latitudes of the North Atlantic with few studies focusing in tropical latitudes where shallow cumulus clouds form (Allan et al., 2008; Behrenfeld et al., 2019; Klingebiel et al., 2019; Rauber et al., 2007; Sorooshian et al., 2020). Shallow cumulus clouds are important for Earth's climate as they are one of the most geographically pervasive cloud types and can influence Earth's radiative budget by reflecting incoming radiation over the low-albedo ocean surface.

Aerosol research conducted in the tropical Atlantic has focused largely~~mostly~~ on the long-range transport of mineral dust from North Africa in the summertime. Long-range African dust transport occurs when emitted desert dust is lofted above the marine boundary layer (MBL) into the Saharan Air Layer (SAL) and is propagated westward (Carlson & Prospero, 1972). As dust is transported westward, it can mix into the underlying moist MBL and deposit into the Atlantic Ocean and Caribbean Sea as well as Western Atlantic land masses such as South America, the Caribbean islands, and North America (Barkley et al., 2019; Carlson & Prospero, 1972; Prospero et al., 1981, 2020). Some studies have attempted to understand the effects of long-range transported dust on cloud droplet formation and water uptake with varying results depending on the degree of aging that dust experiences during transport (Allan et al., 2008; Denjean et al., 2015; Kristensen et al., 2016; Rosenfeld et al., 2001; Wex et al., 2016). However~~Ultimately, though~~, these studies provide conflicting results on whether dust particles are hygroscopic and numerous enough to appreciably impact CCN concentrations ~~and, as a resultthus, do not thoroughly explain aerosol-cloud interactions~~ in the tropical Atlantic. Due to the annual oscillation of the intertropical convergence zone (ITCZ), dust transport also exhibits a seasonality in terms of its geographic extent (Adams et al., 2012; Chin et al., 2014; Prospero & Lamb., 2003; Prospero, 1968; Prospero & Mayol-Bracero, 2013; Yu et al., 2019; Zuidema et al., 2019). However, marine shallow cumulus clouds form year-round in the tropical Atlantic regardless of dust transport. Thus, it is important to focus on aerosol characteristics across a full seasonal cycle to obtain a thorough understanding of the role aerosols play on cloud formation in the tropical Atlantic ~~, suggesting that other marine or other long-range transported sources are important for aerosol-cloud interactions in this region~~ (McCoy et al., 2022).

Few studies have attempted to fully understand which aerosols are the most prominent CCN ~~both~~ during both the boreal summer (when dust concentrations are at a maximum)~~dust seasons~~ and boreal winter (when dust concentrations are at a minimum)~~non-dust seasons~~ in the tropical North Atlantic MBL. African smoke is o~~O~~ne particle type that may be important for CCN activation in the tropical N~~n~~orth Atlantic, yet has been understudied at dust receptor sites like~~such as~~ Barbados ~~is African smoke~~ (Wex et al., 2016). In contrast to dust, previous research has shown that smoke particles are an important source of CCN (Edwards et al., 2021; Lathem et al., 2013; Pierce et al., 2007; Spracklen et al., 2011) with more recent research showing that some smoke particles can activate at supersaturations as low as 0.05% (Rogers et al., 1991).

There are a number of reasons that explain why smoke particles can be effective CCN. Smoke particles are often complex mixtures of both organic and inorganic components that change compositionally and morphologically during their residence time in the atmosphere (Cappa et al., 2020; Hodshire et al., 2019; Konovalov et al., 2021; Reid et al., 2005; Wu et al., 2021). Smoke properties may also vary between fires depending on fuel type and moisture, combustion phase, wind conditions, etc. (Andreae, 2019; Miles et al., 1995; Reid et al., 2005). In general, smoke particles are often found in the accumulation mode of the aerosol size distribution and primarily contain particulate organic matter, black carbon, and inorganic components including potassium chloride salts (Reid et al., 2005). Upon emission, smoke can undergo chemical processing through photochemical and heterogeneous reactions, including the loss of chloride and acquisition of sulfate and nitrate, creating potassium sulfate compounds in smoke that are often used as tracers of aged smoke and can affect the hygroscopicity of smoke particles (Capes et al., 2008; Hennigan et al., 2010, 2011; Reid et al., 2005; Zauscher et al., 2013). Chemical processing can also lead to morphological changes as the condensation of gaseous compounds and multiphase processes with aqueous compounds can result in the growth and sphericity of smoke particles, which in turn can affect the CCN properties of smoke particles~~smoke particles~~ (Abel et al., 2003; Giordano et al., 2015; Reid et al., 1998; Zhang et al., 2008). The ~~many~~ variations ~~and changes~~ in the chemical and physical properties of emitted smoke particles as well as the changes these properties can undergo in transit ~~during their residence time in the~~ make it difficult to predict the ability of smoke particles ~~atmosphere makes it difficult to study these particles thoroughly and can also affect their ability~~ to act as CCN.

In this study, we investigated the relationship between submicron aerosol composition and CCN in the tropical N~~n~~orth Atlantic MBL during marine background conditions and conditions affected by long-range continental aerosol transport of smoke and dust particles (henceforth referred to as "CAT" conditions). To perform this work, we collected aerosol samples and size-resolved CCN data from January to February 2020 at the Barbados Atmospheric Chemistry Observatory (BACO) during the Elucidating the Role of Clouds–Circulation Coupling in Climate/Atlantic Tradewind Ocean-Atmosphere Mesoscale Interaction Campaign (EUREC^{4}A/ATOMIC) campaigns (Quinn et al., 2021; Stevens et al., 2021). Conducting this research during the boreal winter provided a unique opportunity to explore aerosol-cloud interactions in~~ different~~ meteorological conditions different from those that~~than~~ are typically studied in the tropical North Atlantic. Dust primarily arrives to Barbados during the summer months with peaks in June and July (Zuidema et al., 2019). As a result, dust receptor sites in Barbados have historically been used to compare CAT and marine background conditions during the boreal summer. During the winter, the southward shift of the ITCZ directs African dust to South America, resulting in a decrease in dust concentrations over Barbados during the winter months with days in December and January sometimes receiving no dust at all (Prospero, 1968; Prospero et al., 2014; Prospero & Lamb, 2003; Prospero & Mayol-Bracero, 2013). However, during the EUREC^{4}A/ATOMIC campaigns, we observed anomalous wintertime transport of African aerosols to Barbados, which provided novel sampling conditions to study the effects of various aerosol types on cloud droplet formation. Specifically, we were able to explore how the addition of continental aerosols like mineral dust and smoke particles to background marine aerosols consisting of organics, sulfates, and sea salt affects CCN activity.~~such as organics, sulfates, and sea salt and how the addition of continental aerosols like mineral dust and~~

~~smoke particles affects CCN activity~~ This allowed us to~~, thus~~ compare~~ring~~ the impact of ocean-derived vs. long-range transported aerosol on water uptake properties and CCN concentrations. We conclude this manuscript by discussing the importance of our findings for cloud formation in the tropical North Atlantic.

Methods

Measurement Site and Sampling Period

Aerosol samples and size-resolved CCN data were collected at the Barbados Atmospheric Chemistry Observatory (BACO) on Ragged Point during the EUREC^{4}A and ATOMIC field campaigns from January 20, 2020 -February 20, 2020 (Quinn et al., 2021; Stevens et al., 2021). Ragged Point (13° 6' N, 59° 37' W), a prominence on Barbados' east coast, is an ideal location for studying the impact of long-range African aerosol transport on aerosol-cloud~~ aerosol~~ interactions as it is situated on the most easterly island in the Caribbean and is exposed to the steady easterly trade winds. Thus, the east coast of the island is subject to little anthropogenic aerosol influence from local islands to the west (Prospero et al., 2005; Savoie et al., 2002). Further, the island is at a latitude coinciding with the outflow of African aerosols such as mineral dust (Carlson & Prospero, 1972; Prospero, 1968) and biomass burning (Archibald et al., 2015) as well as tropical marine cumulus clouds (Stevens et al., 2016).

Air Mass Origins

During the sampling period, air masses of varying compositions were observed at Ragged Point. To determine the origin of these air masses, 150 h back trajectories were generated every 6 ~~hours (~~h~~)~~ at heights of 500, 1000, and 1500 ~~meters (~~m~~)~~ throughout the campaign using the Hybrid Single Particle Lagrangian Integrated Trajectory (HYSPLIT) model calculated using model vertical velocity and meteorology from the National Center for Environmental Prediction (NCEP) 1-degree Global Data Assimilation System (GDAS) (Rolph et al., 2017; Stein et al., 2015).

Dust Concentration

To collect aerosols, BACO is equipped with a high-volume sampler and an isokinetic aerosol inlet on top of a 17 m tall tower situated on a 30 m bluff along the coast at Ragged Point. Daily dust mass concentrations were determined from filter-based measurements (Prospero et al., 2021; Zuidema et al., 2019) using a high-volume air sampler pumping at a rate of approximately 0.7 m^3/min across a 20 cm x 25 cm cellulose Whatman-41 (W-41) filter with a nominal 20 µm pore size. W-41 filters were chosen for this analysis as they allow for high flow rates and yield a collection efficiency of 95% or better for dust (Kitto & Anderson, 1988) and submicron aerosols (Pszenny et al., 1993). Upper particle diameter limits for W-41 filters with 20 µm pore size are approximately 80-100 µm or greater (Barkley et al., 2021). After aerosol collection, the filters are washed with milli-q water three times to remove soluble material then placed in a furnace and combusted at 500°C for about 12 hrs. (i.e., overnight). Procedural blanks are also collected by placing a filter in the sampler for 15 minutes without turning on the pump. The resulting ash mass from a sample minus the mass of a filter blank is the gross ash weight, which is then adjusted by a factor of 1.3 to convert the ash weight to a approximate amount of mineral dust concentrationcollected on the filter during the sample period. Previous research has confirmed the validity of this method for determining dust mass concentrations through chemical analysis of dust ash determined from filters collected in Barbados, crustal abundance, and soil dust composition (Zuidema et al., 2019). A correction factor of 1.3 is applied to the calculated dust concentrations to account for dust components such as bound water or soluble ions that are lost during the heating process (Prospero, 1999; Zuidema et al., 2019).

Aerosol Chemical Composition

Aerosol particles were sampled at ambient relative humidity (RH) through an isokinetic aerosol inlet and collected using a three-stage microanalysis particle sampler (MPS-3, California Measurements, Inc.), which samples particles from diameters of 5.0-2.5 µm (stage 1), 2.5 µm – 0.7 µm (stage 2), and <0.7 µm (stage 3). For each set of samples (1 set including 1 sample from each stage of the MPS), the MPS was run for 45 min at 2 L/min flow starting at approximately 9:30 local time or 13:30 coordinated universal time (UTC). Meteorological data from a local station was also used to manually check that wind direction fell between 335° and 130° and wind speeds were greater than 1 m/s during all sampling periods. Sampling during these wind conditions ensures that only air from the open ocean was sampled rather than local, anthropogenically-influenced air.

To determine aerosol chemical composition, p~~P~~articles were deposited onto carbon-coated copper grids (Ted Pella, Inc.) that were later analyzed at the Pacific Northwest National Laboratory using computer-controlled scanning electron microscopy coupled with energy dispersive x-ray spectroscopy (CCSEM/EDX; Quanta 3D) to determine the elemental composition of individual particles. We also collected samples on silicon wafers (Ted Pella, Inc.) which were analyzed with CCSEM/EDX to confirm the vailidity of the carbon measurements on the carbon-coated copper grids. Here, we focus only on the submicron particle population which exerts a greater influence on CCN number concentrations and is more sensitive to chemical changes that affect~~s~~ its hygroscopicity. Thus, for this study we focus primarily on~~only present~~ data from stage 3 of the MPS, representing <0.7 µm diameter particles.

CCSEM/EDX is a valid method for determining size-resolved chemistry of the aerosol loading as CCSEM excels in calculating particle size by imaging individual aerosols while EDX provides the relative abundances for elements of interest (Tomlin et al., 2021). considered a semiquantitative method providing the relative atomic fractions for elements of interest. Percent composition threshold values of 1% were used to ensure the presence of elements detected by the EDX. Single-particle analysis using Elements of interest in CCSEM/EDX analysis wasere limited to 16 common elements indicative of organic material, sea spray, dust, and anthropogenic emissionsfound in common aerosols such as dust, sea salt, and smoke particles: carbon (C), nitrogen (N), oxygen (O), sodium (Na), magnesium (Mg), aluminum (Al), silicon (Si), phosphorus (P), sulfur (S), chlorine (Cl), potassium (K), calcium (Ca), vanadium (V), manganese (Mn), iron (Fe), and nickel (Ni). The EDX peak for Cu is heavily influenced by -thea background signal from the Cu grid and is excluded from analysis. Samples collected on Si substrates confirmed the validity of the C signal in analyzed particles, as the carbon coating on the Cu substrates has the potential to generate a background signal as well. An excess of 1000 particles were analyzed in each sample. Due to size limitations of the CCSEM, only particles with diameters >0.1 µm were analyzed. Data products from CCSEM/EDX analysis were then analyzed in MATLAB (ver 9.6.0; The Mathworks, Inc.) using a K-means clustering algorithm (Ault et al., 2012; Shen et al., 2016). The algorithm operates by generating categories of similar particles (clusters) based on the presence and intensity of elemental peaks in individual single-particle EDX spectra. These clusters are then assigned to particle types based on their size, morphology, characteristic EDX spectra, and existing literature. A more thorough explanation of the k-means clustering algorithm and particle identification process including the plots used to perform particle identification (Figure S1) is provided in the Supporting Information (SI).

~~Particle types typically observed in the supermicron aerosol loading, such as sea salt and dust, are not as abundant in our samples as we focus exclusively on the submicron aerosol loading.~~

Size-Resolved CCN Measurements and Data Analysis

To determine the size-resolved CCN activity of aerosol particles during the sampling period, we used a continuous-flow streamwise thermal gradient CCN counter (CCNC, model CCN-100, DMT, Longmont, Co, USA; (Roberts & Nenes, 2005; Rose et al., 2008)) combined with a differential mobility analyzer (DMA, modified model M, Grimm Aerosol Technik, Ainring, Germany) and condensation particle counter (CPC, model 5412, Grimm Aerosol Technik). The method is described in detail in Pohlker et al 2016. Flows for the size-resolved CCN set-up included a sheath:sample flow ratio of 10 for the CCN counter (sample~~total~~ flow rate of 0.5 L/min), a sheath flow of 8 L/min for the DMA, and a sample flow of 0.6 L/min for the CPC. Upon entering the system, the sampled air was dried using a condensation drier to maintain a relative humidity (RH) between 20 and 30% and to ensure reliable hygroscopicity measurements. After drying, the particles passed through a DMA which selected particles with a diameter (D) between 20 and 245 nm. The monodisperse aerosol-laden flow was then split between the CCNC and CPC. Inside the CCNC, the particles were subjected to ~~water vapor~~ supersaturations (S) of~~including~~ 0.09, 0.16, 0.24, 0.43, and 0.74 %.

Formatted: Indent: First line: 0"

Calibrations of the CCNC supersaturations were performed according to the method described in Rose et al. 2008 by generating and size-selecting ammonium sulfate particles that were analyzed by the CCNC set to a designated temperature gradient as well as a CPC to measure total condensation nuclei (CN) values. Plots comparing CCN/CN and dry particle diameter were then used to determine the diameter at which 50% of the particles in an aerosol population activate as CCN at a particular S, also called the critical activation diameter (d_{50}). D_{50} values were then used to determine supersaturation. Supersaturations were plotted against the designated temperature at the calculated supersaturation. The resulting plot provided a linear curve that could be used to adjust the supersaturation shown by the instrument to the actual value of the column supersaturation. After calibrating, S values averaged 0.08, 0.15, 0.23, 0.41, and 0.71 %1.

For ambient sampling, particles that activate as CCN at each S and D are counted in the CCNC as CCN, while all particles of a selected D are counted in the CPC to determine the total aerosol concentration of particles at each D. By scanning D at a given value of S, measurements from the CPC and CCNC are then used to generate an activation curve used to calculate the d_{50}. These values, along with the particle number size distribution determined by a scanning mobility particle sizerthe SMPS, (SMPS, TSI model 3080 with CPC 3772) operating independently of the CCNC setup, are then used to calculate the activation curve and the effective hygroscopicity parameter κ using equation (1) according to the κ-Köhler model (Petters & Kreidenweis, 2007):

$$\kappa = \frac{4A^3}{27D_p^3 \ln^2 S_{crit}} \quad (1)$$

where D_p is the dry particle diameter, S_{crit} is the supersaturation set by the CCN counter, and A is the Kelvin term calculated from equation (2):

$$A = \frac{4\sigma M_w}{RT\rho_w} \quad (2)$$

Where σ is the surface tension (σ=0.072 J/m^2), R is the universal gas constant, M_w is the molecular weight of water, and ρ_w is the density of water. In the κ-Köhler model, higher values of κ indicate a more hygroscopic particle that is more efficient at taking up water and can activate as CCN at lower S. ~~Calculations of activation curves, size-resolved CCN, CCN efficiencies, and errors are described in detail in~~ Pöhlker et al. 2016~~.~~

Results and Discussion

In this section we will show that, ~~We find that,~~ upon arrival of co-transported dust and smoke, smoke originating from fires in the African Sahel dominate the accumulation mode particle population in the tropical North Atlantic MBL, which results in an increase in CCN number concentration. Though dust and smoke are both transported to the region, smoke dominates the accumulation mode number concentration by an order of magnitude compared to dust. These findings are supported by data products from dust mass concentrations, size-resolved hygroscopicity, single particle data (~~e.g.,~~ CCSEM-EDX), and air mass history (~~e.g.,~~ NOAA'S HYSPLIT model), which all complement one another and provide unique insights into the aerosol sources, their single particle composition, and their effects on cloud droplet activation.

Air Mass Characteristics~~Sampling Conditions~~ during the EUREC^{4}A and ATOMIC Campaigns

To confirm the origins of the various air masses sampled, we performed back trajectory analysis throughout the campaign using NOAA's HYSPLIT model (Figure 1) and quantified dust mass concentrations (Figure 2a). Results of these two analyses show that Barbados was influenced by two types of air masses during the sampling period: air masses that, over the course of 6 days, do not pass over land (referred to as clean marine conditions), and air masses that have passed over the African continent ~~influenced by continental regions~~ (referred to as continental aerosol transport (CAT) events).~~ To confirm the origins of the various air masses sampled, we performed back trajectory analysis throughout the campaign using NOAA's~~

HYSPLIT model. Back trajectory analysis was not conducted for time periods longer than 6 days, which introduces the possibility that marine air masses could have been influenced by European outflow as well. Figure 1 shows that during periods with low dust mass concentrations and a bimodal size distribution, air masses originated from the remote Atlantic Ocean at higher latitudes with no land contact over 6 days. Influence from European outflow during these time periods may be present, but likely is minimal. During time periods with high dust mass concentrations, air masses originated from continental Africa. Figure 2a shows that the total mass concentration of dust particles correlates very well with the arrival of air masses originating from Africa. During time periods when dust concentrations were low, the particle loading has a bimodal size distribution characteristic of clean marine air masses in which the accumulation mode is composed primarily of sulfates, while the Aitken mode is composed primarily of organics (Figure 2b) (Ault et al., 2013; Hoppel et al., 1986; O'Dowd et al., 2004). Upon the increase in dust mass concentrations, the submicron particle size distribution correspondingly becomes unimodal and the smallest Aitken size mode is negligible, suggesting that long-range transported (LRT) particles are either dominanttoverwhelme overing the background marine particle loading or that smaller Aitken mode particles are coagulating onto larger LRTtransported continental aerosols to form a unimodal accumulation mode (Tomlin et al., 2021).

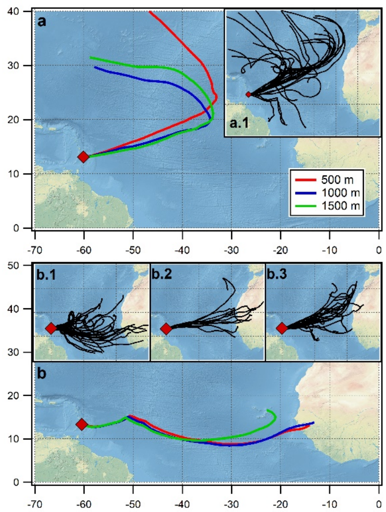

Figure 1: HYSPLIT back trajectories at Ragged Point, Barbados (red diamond) for the EUREC^{4}A/ATOMIC field campaign. (a) Back trajectories for 2020/2/8 18:00 UTC at heights of 500 m (red), 1000 m (blue), and 1500 m (green) exemplify air mass origins during clean marine sampling conditions. Subplot a.1 shows all back trajectories from clean marine sampling conditions collected at 6 h intervals with a release altitude of 1000 m from 2020/1/29 0:00 – 2020/1/29 12:00, 2020/2/6 12:00 – 2020/2/9 18:00 and 2020/2/12 12:00 – 2020/2/15 6:00 UTC. (b) Back trajectories for 2020/2/2 18:00 UTC at 500 m, 1000 m, and 1500 m exemplify air mass origins during CAT conditions. The subplots, b.1, b.2, and b.3 show all back trajectories for 3 time periods during which continental aerosols were sampled: b.1) ~~, including~~ 2020/1/29 18:00 – 2020/2/6 6:00, b.2) 2020/2/10 0:00 – 2020/2/12 6:00, and b.3) 2020/2/15 12:00 – 2020/2/20 18:00 UTC. Trajectories for b subplots were also collected at 6 h intervals with a release altitude of 1000 m.

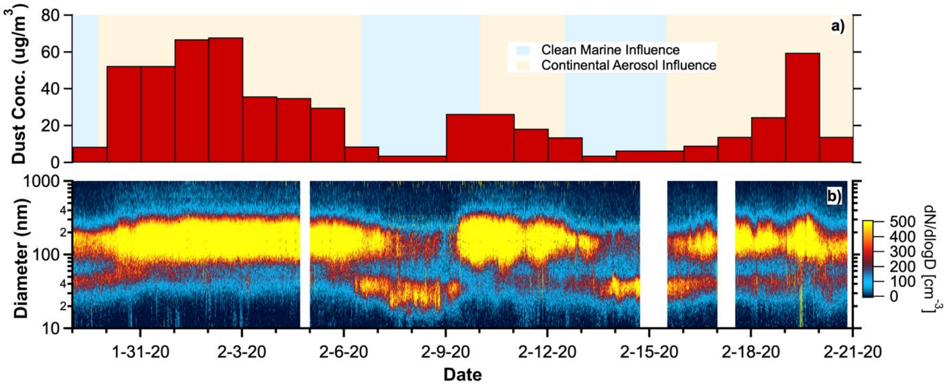

Figure 2 – Temporal evolution of (a) dust mass concentrations determined from bulk aerosol filter samples and (b) submicron aerosol particle size distributions determined with an SMPS. Time for both plots is given in UTC (-4 h local Atlantic Standard Time). Color shading in (a) represents continental aerosol influence (orange shading) and clean marine influence (b) as determined by NOAA HYSPLIT back trajectories calculated at Ragged Point.

Single Particle Aerosol Composition

CCSEM/EDX analysis from the EUREC^{4}A and ATOMIC campaigns revealed the presence of several particle types with distinct chemistries and morphologies in the submicron aerosol loading ~~with distinct morphologies and chemistries~~ (Ault et al., 2014; Behnke et al., 1997; Gaston et al., 2011a, 2013a) ~~during the EUREC^{4}A and ATOMIC campaigns~~. Figure 3 presents SEM images (left) and EDX spectra (right) for each particle type detected on stage 3 of the MPS (particle diameter <0.7 µm), including sea spray, aged sea spray, mineral dust, internally mixed mineral dust and sea spray, sulfate, smoke, internally mixed mineral dust and smoke, and organics. Sea spray particles as well as internally mixed mineral dust and sea spray particles were~~as a~~ dominant components of the supermicron aerosol loading but are~~is~~ only~~ a~~ minor components of submicron aerosol.~~.~~

Sea Spray

Sea spray particles were characterized by high relative abundance of approximately equal parts Na and Cl, indicating the formation of halite (NaCl). Morphologically, sea spray particles have a cubic shape that represents the crystal structure of halite. Small Mg peaks approximately 10% of the height of Na peaks were also observed in NaCl particles and reflect the Na:Mg ratio of seawater. Additional components of sea spray particles include rod-shaped particles containing Ca and S (presumably ~~CaSO4~~calcium sulfate) that were often found attached to NaCl particles (Ault et al., 2013; Bondy et al., 2018; Choël et al., 2007). Elements such as N and S that may suggest aging of sea spray were either absent or present in small relative abundance on NaCl components of sea spray particles. Click or tap here to enter text.

Aged Sea Spray

Aged sea spray was defined by the presence of sea salt components including Na, Mg, K, S, and Cl. In contrast to freshly emitted sea spray particles, aged sea spray has a characteristically low or absent Cl signal with a strong presence of N or S. Figure 3 provides an example of an aged sea spray particle in which Na is high (indicating the presence of salt), but with a low Cl peak (suggesting the particle has been aged). The presence of S in this spectrum may explain the low relative abundance of Cl compared to Na. ~~-~~Sea spray can be aged through reactions with sulfuric acid (H_2SO_4), dinitrogen pentoxide (N_2O_5), and/or nitric acid (HNO_3) which results in Cl depletion and S or N enrichment (Ault et al., 2014; Ault, Guasco, et al., 2013; Behnke et al., 1997; Gaston et al., 2011, 2013; Sobanska et al., 2003). Morphologically, aged sea salt particles had either a similar appearance to fresh sea salt particles, which is often either cubic (as seen in Fig 3), or appeared as a flakey amorphous mass (Hoffman et al., 2004; Laskin et al., 2012; Li et al., 2010).

Mineral Dust

Mineral dust is characterized by the presence of aluminosilicate elements such as Si, Al, Fe, K, Ca, and Mg in EDX spectra, which is consistent with previous studies of African dust (Denjean et al., 2015; Hand et al., 2010; Krueger et al., 2004; Levin et al., 2005; Twohy et al., 2009). Elements such as S and N were not observed in this particle type (Kandler et al., 2018) suggesting that detected dust had~~did~~ not undergone chemical processing during transport. ~~Morphologically, d~~Dust often appeared as a flakey or nodular amorphous mass as exhibited in Fig 3 and previous literature (Krueger et al., 2004; Laskin et al., 2005; Pachauri et al., 2013; Remoundaki et al., 2011).

Internally Mixed Mineral Dust and Sea Spray

Particles containing elements indicative of both mineral dust (Si, Al, Fe, K, Ca, and Mg) and sea salt (approximately equal relative abundances of Na and Cl) were characterized as internally mixed mineral dust and sea spray (Choël et al., 2007; Deboudt et al., 2010; Sobanska et al., 2014). Elements such as S and N were often not present in this particle type, suggesting the particles had not undergone atmospheric aging during transit. Particles containing both dust and sea spray components often appeared as conglomerates of multiple particles with some parts containing more sea spray components and others containing more mineral dust components.

Sulfate

Sulfate-rich particles are a prevalent component of marine submicron aerosol (O'Dowd & de Leeuw, 2007) and characterized here by a dominant S component - often with high relative abundance of~~strong~~ C, O, and N. These particles are likely sulfates bound to NH_4^+ such as ammonium sulfate ($(NH_4)_2SO_4$) or ammonium bisulfate (NH_4HSO_4) (Hand et al., 2010). The high relative abundance of~~strong~~ C~~ component~~ indicates a large organic fraction as well. The morphology of sulfate particles appeared smooth and spherical as reported in previous literature (Nájera & Horn, 2009).

Smoke

Smoke particles were identified by the presence of C with K and S likely representing internally mixed organic and black carbon with potassium-containing salts. K is a well-known indicator for biomass burning (Andreae, 1983; Hand et al., 2010; Hudson et al., 2004; J. Li et al., 2003; Murphy et al., 2006; Pósfai et al., 2003), especially in flaming conditions in Savannah fires as opposed to smoldering conditions (Echalar et al., 1995; Maenhaut et al., 1996). Morphologically, smoke particles can be spherical due to aging or coatings but can also appear as aggregates or chains of spheroids (Dang et al., 2021; Hand et al., 2010; Miller et al., 2021; Pósfai et al., 2003). In this study, smoke particles most frequently appeared as small spherical particles.

Internally Mixed Mineral Dust and Smoke

Internally mixed mineral dust and smoke particles are characterized by dust components such as Si, Al,~~ Mg,~~ Fe, Ca, and Mg with strong contributions of K, S, C, and O. Morphologically, internal mixtures of dust and smoke appear as aggregates of amorphous dust particles with clusters or spheres representing soot from smoke. Single particle chemical analysis of these particles show~~s~~ distinctions between the dust and smoke portion of the particle, with the dust portion having typical dust components (Si, Al,~~ Mg,~~ Fe, Ca, and Mg) and the smoke portion having typical smoke components (K and S with C and O). Previous research has observed internal mixing of carbonaceous particles and dust particles in Africa when significant amounts of both biomass burning and dust were present (Hand et al., 2010); however, we show that these internal mixtures can be transported all the way to the Caribbean as well.

Organics

Organic particles are defined by strong signals of C and O with few other elements present, if any (Hand et al., 2010). The absence of S or N, which are often indicative of sulfate and nitrate, respectively, suggests that these particles have undergone minimal chemical aging. ~~This scarcity of additional elements includes S and N that, if present, would be indicative of sulfate and nitrate, respectively. ~~Morphologically, organic particles are characterized as small individual spheres. The organics were likely marine in origin (Russell et al., 2010) as they were the smallest particle type observed both during clean marine conditions and during CAT conditions, which indicates they may be a "background" aerosol type (Russell et al., 2010).

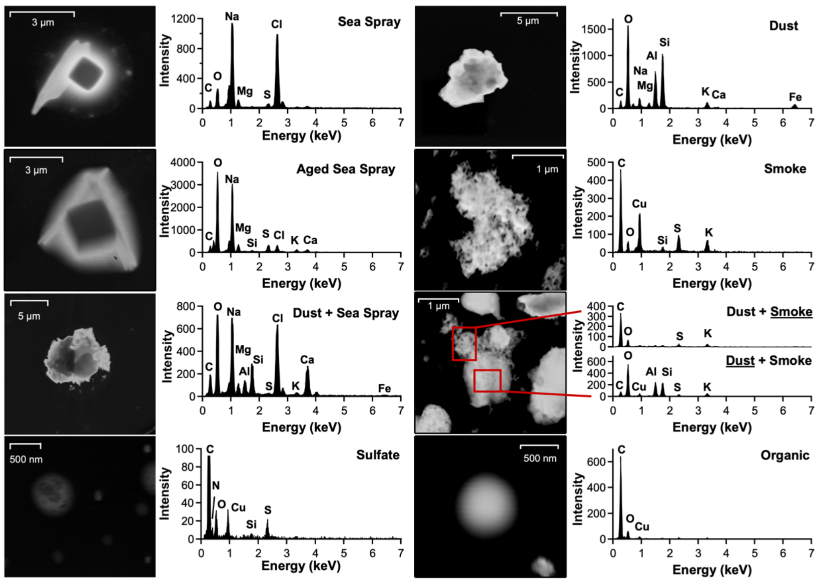

Figure 3: Characteristic aerosol particle types observed by means of SEM-EDX images (left) and spectra (right) in samples collected during the EUREC[4]A/ATOMIC campaign. SpectraPlots for the Dust + Smoke particle type rerepresent different areas analyzed on the particle with EDX, denoted by the red boxes.

Arrival of Anomalous Wintertime Co-Transported Dust and Smoke

Figure 4 presents number fractions for particles detected in the submicron aerosol loading throughout the sampling period and reveals a similar trend in smoke particle number fractions to those of dust mass concentrations in Figure 2, suggesting that smoke and dust were co-transported to Barbados from Africa. A similar plot to Figure 4 that contains temporal chemistry from stage 1 and stage 2 of the MPS (representing supermicron particles ><0.7 µm diameter) determined using CCSEM/EDX analysis can be found in the SI (Figure S2). During the boreal winter, the Sahel region in North Africa experiences its fire season in which large swathes of land are burned and large plumes of smoke are emitted from the region (Figure S3;(Ansmann et al., 2009; Barkley et al., 2019; Roberts et al., 2009). However, due to the southward shift in the ITCZ during ~~the~~ boreal winter, smoke is expected to be transported primarily to South America (Moran-Zuloaga et al., 2018; Talbot et al., 1990; Wang et al., 2016). In our study, we observed the arrival of this smoke on Barbados. These findings are supported by temporal carbon monoxide (CO) column density measurements that are often used as a tracer for smoke (Figure S4 and S5). Periods that correspond to clean marine influence ~~in the HYSPLIT model from Figure 1 and low bulk dust mass concentrations in Figure 2~~ are dominated by sulfate and organic particles in the submicron aerosol ~~as exhibited in~~ (Figure 4). Upon arrival of continental aerosols ~~as shown in Figure 1 and Figure 2 (2020/1/29 – 2020/2/7, 2020/2/9 – 2020/2/12 – 2020/2/16 – 2020/2/20 UTC),~~ ~~that correspond with continental aerosol influence from the HYSPLIT model and bulk dust concentrations (2020/1/29 – 2020/2/7, 2020/2/9 – 2020/2/12 – 2020/2/16 – 2020/2/20 UTC),~~ wildfire smoke appeared~~s~~ to dominate~~overwhelm~~ the number fraction of ~~the~~ submicron aerosol ~~loading~~.

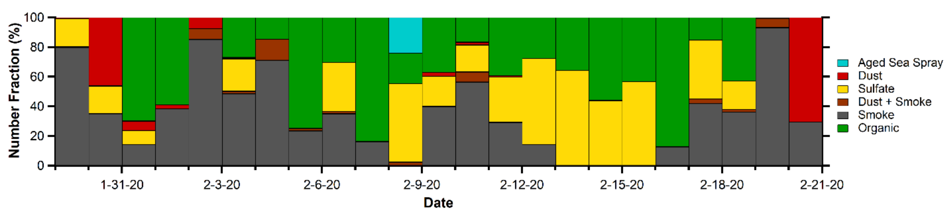

Figure 4: Temporal evolution of submicron number fractions for different types of aerosol particles determined by CCSEM/EDX analysis. The total number of particles analyzed for each day ranges from 1000 to 20,000.

Figure 5 presents ~~provides a detailed~~ size-resolved chemical data from CCSEM/EDX analysis from clean marine periods (average of all clean marine periods) and one exemplary time period influenced by continental air masses (CAT event 1). Similar plots for other CAT events are provided in the SI (Figure S6). Average particle diameters for each particle type during each sampling period are~~is~~ also provided in Table S1. ~~size-resolved plot of single particle chemistry from both clean marine periods (clean marine), and periods that were influenced by air masses from continental Africa (CAT event 1). Analysis of other CAT events (Figure S4) show similar chemical trends to those shown in the Cat Event 1 plot.~~ Figure 5 shows that in ~~both~~ clean marine periods ~~and CAT events~~, a small fraction of large particles have both a smoke and a dust signature. This suggests that our “clean marine conditions” are only “clean” relative to time periods dominated by dust and smoke, rather than pristine clean marine conditions without any continental aerosol influence. ~~Both the clean marine~~ The~~and~~ CAT event plot in Figure 5 demonstrates that dust as well as~~and~~ internally mixed dust and smoke particles dominate~~tend to be the largest particle types~~ in the submicron aerosol loading, followed by smoke. ~~Even in nominally clean marine periods, there is still a substantial contribution of dust, smoke, and internally mixed dust and smoke, especially at larger sizes. This suggests that our “clean marine conditions” are only “clean” relativecompared to time periods dominatedinfluenced by dust and smoke, rather than pristine clean marine conditions without any continental aerosol influence.~~ Smoke particles follow as the next largest particle type. Organics dominate in the smallest size fractions, followed by sulfates, ~~The smallest particle types were found to be organics followed by sulfates~~ suggesting a ~~primary emission of marine organics and a~~ secondary source for sulfate (Bates et al., 1992). Aged sea salt particles were on average smaller than most dust, internally mixed dust and smoke, and smoke particles. Figure 5~~4~~ also shows that at a diameter of ~0.1µm (which is approximately the d_{50} of CCN at S 0.16% in clean marine conditions and ~~conditions influenced by continental aerosol transport~~CAT conditions) the composition~~chemistry~~ is dominated by sulfates and organics in the clean marine conditions, while smoke and organics dominate in the CAT event. The~~A~~ large decrease in sulfate number fraction during CAT events might be caused by the condensation of Aitken mode sulfate-containing particles onto larger, long-range transported particles as indicated in Fig. 2 (Gaston et al., 2010).~~suggests that marine biogenic sulfur precursors are condensing onto larger transported particles and might explain the loss of the Aitken mode observed in Figure 2.~~

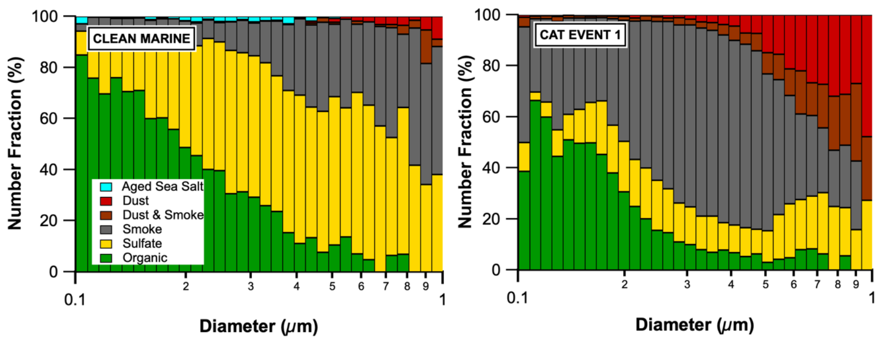

Figure 5: Number fractions of different types of submicron aerosol particles plotted against particle diameter. The "clean marine" plot (left) includes data from all clean marine sampling periods. The "CAT Event 1" plot (right) includes data from the first period in which dust and wildfire smoke were observed over Barbados (2020/1/29 18:00 – 2020/2/6 6:00 UTC). Particles were organized into 32 size cuts (bins) to maximize resolution of size-resolved chemical data. Particle counts in each bin range from 34 particles to up to 3041 with an average bin count of 493 particles for the Clean Marine plot and 973 for the CAT Event plot.~~Bin sizes for each decade~~

can range from 34 particles to up to 3041 with an average bin size of 493 particles for the Clean Marine plot and 973 for the CAT Event plot.

Changes in Aerosol Hygroscopicity during EUREC^{4}A/ATOMIC

Comparisons between size-resolved CCN measurementsκ and submicron single particle elemental composition reveal that smoke particles lower the hygroscopicity of the submicron aerosol loading hygroscopicity compared to marine-derived submicron aerosol in the tropical North Atlantic. Figure 6 presents boxplots for κ values as well as average d_{50} measured at each S during both clean marine conditions and CATdusty conditions. Clean marine and CAT conditions are determined by data from HYSPLIT back trajectory analysis and dust mass concentrations and are described in detail in Table 1. Both plots show a similar trend in which average κ increases from 0.09% S to 0.24% S. Then, with each subsequent increase in S after 0.24% S, κ decreases as smaller, less hygroscopic particles activate at higher supersaturations. The low hygroscopicity of these smaller particles can be explained by compositional changes in the aerosol loading exhibited in Fig 5, reflecting the shift in particle chemistry from mostly sulfate to mostly organic with decreasing particle size likely due to smaller, less hygroscopic particles activating at higher supersaturations. Also of note is the κ of 0.6 observed for clean marine conditions at 0.24% S, which matches κ measurements for ammonium sulfate particles that can dominate along with sea spray organics during clean marine conditions (Petters & Kreidenweis, 2007).

Formatted: Font: Symbol

There is also a noticeable drop in average κ between the same supersaturations in clean marine conditions compared to CATsmokey conditions. For example, at 0.16% S, κ=0.52±0.09 for all clean marine condition periodss and κ=0.46±0.10 for all continental aerosol transport periods. This is likely due to the addition of less hygroscopic material such as dust and smoke particles that ~~are acting as CCN and~~ are not ~~present~~ dominant in clean marine conditions. As expected, trends in average d_{50} for both plots indicate that smaller particles activate as CCN with larger supersaturations.~~As expected, trends in average d_{50} for both plots show that activation diameters decrease with an increase in supersaturation, indicating that smaller particles activate as CCN with larger supersaturations.~~ Activation diameters during CAT conditions are also larger than corresponding activation diameters in clean marine conditions for the same supersaturation. This also suggests that the addition of less soluble material from transported smoke particles lowers the hygroscopicity and increases the activation diameter.

When comparing hygroscopicity data from this study to previous research, we find both similarities and differences in κ trends. For example, Good et al. 2010 presents data collected in the tropical eastern Atlantic that provides an ideal comparison to our findings. On average, their values for κ in clean marine conditions and during observations of dust transport (κ=1.15-1.4 and 0.8-0.92, respectively) were much higher than our observed values. However, Good et al. 2010 shows similarities to our work through the distinct drop in κ between clean marine conditions and CAT conditions, which is attributed to the addition of hydrophobic dust to the aerosol loading. ~~However, one finding of note from~~ Click or tap here to enter text. ~~is the distinct drop in κ between clean marine conditions and conditions influenced by continental aerosols from Africa owing to the addition of more hydrophobic particles such as dust that activate as CCN. Our data shows a similar drop in κ from clean marine conditions to conditions influenced by long-range transported~~ Wex et al. 2016 present CCN data from ground-based field sampling ~~of CCN data~~ in November and April at Ragged Point, Barbados. They show a similar trend in κ in which values increase from 0.1% S, peak at 0.2% S, then decrease with each subsequent increase in S. They

Formatted: Font: Times, 12 pt

Formatted: Font: Symbol, 12 pt

Formatted: Font: Times, 12 pt

Formatted: Font: Times, 12 pt

Click or tap here to enter text.~~-~~also found a similar drop in κ upon the arrival of long-range transported aerosols, likely due to less hygroscopic particles from continental sources activating as CCN. A separate study from Kristensen et al. 2016 conducted similar research at Ragged Point, Barbados during the boreal summer. The range in κ values of 0.2-0.5 match those observed in our work, especially during CAT events. However, Kristensen et al. 2016 determined that concentrations of dust, sea salt, and soot were too small to influence CCN, concluding that sulfates and organics were the primary CCN types. They conclude that the low κ values observed during their sampling were due to organic compounds activating as CCN. We find similar κ values to Kristensen et al. 2016 and a similar particle chemistry of the accumulation and Aikten modes during clean marine conditions, suggesting that organics and sulfates were the primary CCN types during clean marine conditions studied for the EUREC4A and ATOMIC campaigns as well. ~~However, w~~We also observe a drop~~this is the case for clean marine conditions but the change in~~ κ from ~~between~~ clean marine conditions to~~and~~ CAT events. This drop in κ indicates the influence of an additional CCN particle type contributed by the CAT events.~~.~~

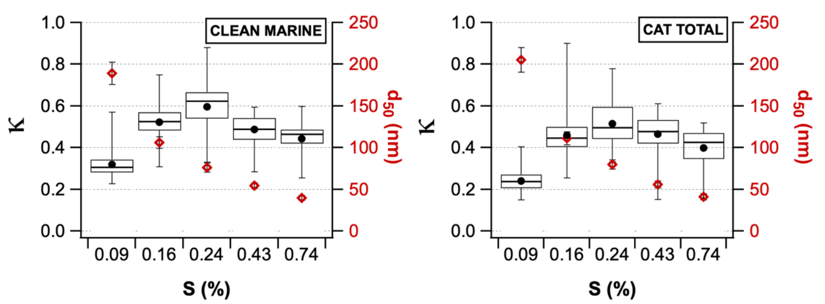

Figure 6: Hygroscopicity parameter κ (left axis, box plots) and corresponding ~~-~~mean diameter at which 50% of the particles in an aerosol population activate as CCN at a particular S,

also called the critical diameter~~critical diameter~~ "d_{50}" (right axis; red markers) for the investigated ~~levels of water vapor~~ supersaturations (S). Whiskers on "d_{50}" markers represent standard deviation values of "d_{50}". Black dots in the boxplot indicate κ mean values. Boxes represent the upper quartile, median, and lower quartile κ values at each S. Whiskers represent the upper and lower limit of κ at each S.

African Smoke Particles Enhance CCN Concentrations

Comparisons between smoke fractions and CCN counts suggest that smoke particles enhance the number of CCN in the tropical North Atlantic MBL. Figure 7 presents two temporal plots of κ (Figure 7a) and smoke number fractions with CCN counts measured at 0.16% S (Figure 7b). Table 1 provides averages of CCN concentrations for each time period shown in Fig.~~ure~~ 7b. Table S2 also provides average and median counts of analyzed smoke particles calculated for each CAT event, including CAT Event 3 which had fewer smoke particles and a higher ~~which may explain the comparatively high hygroscopicity~~κ compared to other CAT Events ~~of CCN during CAT Event 3~~. Figure 7~~a~~ suggests that there is an inverse relationship between κ and smoke number fractions in which an increase in smoke particles results in a decrease in κ. This is likely due to the activation of smoke particles as CCN, which are on average less hygroscopic than the sulfate particles that act as CCN during clean marine conditions. Figure 7b shows a positive correlation~~In Fig 7b, there is a clear and direct relationship~~ between smoke number fractions and CCN counts. A correlation plot of smoke number fraction and CCN concentrations is also provided in Figure S7 to further emphasize their direct relationship.

Formatted: Font: Symbol

There are multiple~~several~~ possible explanations for why African smoke particles may have acted as CCN. As shown in Figure 5, smoke particles are larger than organics and sulfates, on average, and dominate~~overwhelm~~ sulfate and organic particle number concentrations upon arrival of long-range transported African aerosols. In this case, the relatively large size of the smoke particles makes for better CCN compared to organics or sulfates via the Kelvin effect (Dusek et al., 2006). ~~The large number of smoke particles overwhelms the particle loading, providing more surface area for water condensation than is available on sulfate or organic particles. Another potential explanation for smoke particles acting as CCN could be the presence of water-soluble organic compounds (WSOC) such as dicarboxylic acids and humic-like substances that increase CCN numbers through the Raoult effect~~ Click or tap here to enter text.~~. In addition to WSOC, aerosols can also contain organic surfactants that decrease surface tension and thus lower the vapor pressure necessary for CCN activation~~ Click or tap here to enter text.~~. Aging of organic components can also potentially explain the ability of smoke particles to activate as CCN. Studies conducted on the aging of organic components show that a higher O:C ratio (a proxy for aerosol organic aging) increases aerosol hygroscopicity~~ Click or tap here to enter text.~~. The long-range transport of smoke particles from Africa to Barbados would theoretically provide ample exposure time of smoke particles to oxidants such that aging of the particles could occur (Jimenez et al., 2009; Massoli et al., 2010). However, studies exploring the aging of biomass burning particles specifically show that aging results in a drop in κ, rather than an increase as observed in aging of secondary organic aerosols~~ Click or tap here to enter text.~~. Finally, t~~he presence of salts in smoke particles has also been shown to be an important component in smoke hygroscopicity and may explain why smoke is efficient as CCN. Previous studies have shown that smoke particles often contain hygroscopic salts such as potassium chloride, potassium sulfate, and potassium nitrate (e.g., KCl, KNO_3, and K_2SO_4) (Dang et al., 2022; Freney et al., 2009; Zauscher et al., 2013). Other research also shows that only small fractions of salts are needed to increase aerosol hygroscopicity (Roberts et al., 2002). Based on CCSEM/EDX analysis, we find evidence that potassium sulfate salts may be present in transported smoke particles, and thus may explain the potential for smoke to act as CCN. ~~Though the comparatively large size of smoke particles and the presence of hygroscopic salts may be sufficient for explaining why smoke particles are viable CCN particles, there are several other potential contributing factors as well. However, this study has limited evidence on these other factors, thus they are beyond the scope of this study.~~~~It is likely that biomass burning hygroscopicity can be explained by a combination of factors. For example, previous research has found that the presence of salts can enhance the surfactant effect of hydrophobic organic compounds~~ Click or tap here to enter text.~~.~~

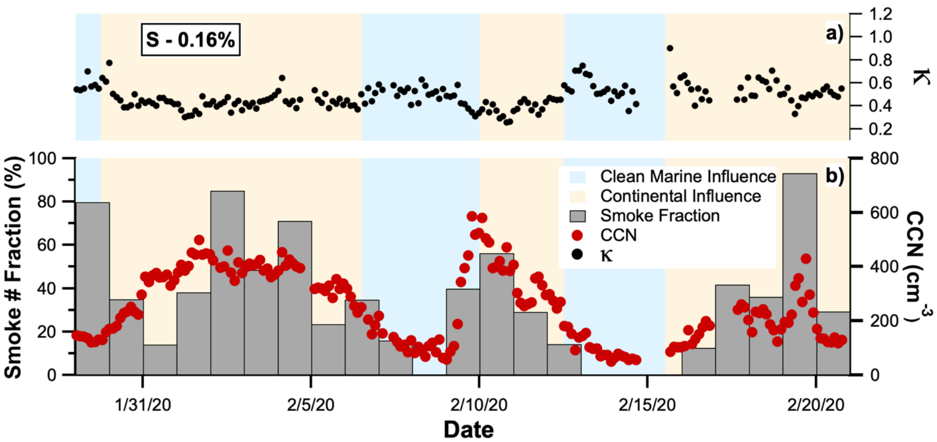

Figure 7: Temporal evolution of hygroscopicity parameter κ (black dots, upper panel) and CCN number concentration (red dots, lower panel), both measured at S = 0.16%, and smoke particle

number fraction (grey bars, left axis, lower panel). Background color shadings indicate periods of continental influence (orange) and clean marine influence (blue) determined by HYSPLIT back trajectories and dust mass concentrations.

Table 1 – Values for average CCN Concentrations and κ measured at 0.16% S during each clean marine influence period and CAT event sampled during the EUREC^{4}A and ATOMIC campaigns.

Sampling Period	**Day/Time**	**CCN Concentrations (pt/cm^3)**	**Average κ**
Clean Marine Period 1	2020/1/29 0:00 – 2020/1/29 12:00	140±10	0.58±0.07
CAT Event 1	2020/1/29 18:00 – 2020/2/6 6:00	340±90	0.44±0.08
Clean Marine Period 2	2020/2/6 12:00 – 2020/2/9 18:00	150±98	0.50±0.10
CAT Event 2	2020/2/10 0:00 – 2020/2/12 6:00	400±106	0.38±0.06
Clean Marine Period 3	2020/2/12 12:00 – 2020/2/15 6:00	100±42	0.55±0.10
CAT Event 3	2020/2/15 12:00 – 2020/2/20 – 18:00	190±75	0.54±0.10

Conclusions

During clean marine conditions, the submicron aerosol loading consists primarily of sulfate and organic particles. CCN measurements determine cloud activation by particles approximately 80 nm in activation diameter with an average κ = 0.52±0.08 for 0.16% S. Comparisons between particle size, hygroscopicity, and single particle elemental composition suggest that sulfate particles (likely ammonium sulfate) are the primary CCN particles in clean marine conditions. During the EUREC^{4}A/ATOMIC campaign, Barbados received three African aerosol transport events during which we detected mineral dust and smoke particles from northern Africa. Upon the arrival of African aerosols to BACO, CCN average activation diameter increased to approximately 200 nm while the average hygroscopicity of activated particles for all CAT events decreased to κ = 0.45±0.1 for 0.16% S. Upon arrival of high concentrations of smoke particles to Barbados, smoke particles dominate~~overwhelm~~ the accumulation mode particle loading, decrease aerosol hygroscopicity, and also increase CCN number concentrations, which could also increase the cloud droplet number concentration and alter cloud radiative properties (Twomey, 1974). Overall, we find that smoke has a large~~r~~ effect on CCN number concentrations ~~than dust does~~ during the boreal winter when smoke transport is high.~~.~~

The observation of smoke transported to Barbados during the boreal winter also indicates the large geographic extent of African smoke that can impact the MBL. Building upon recent work from Ragged Point and other parts of the tropical and subtropical Atlantic (Holanda et al., 2020; Kacarab et al., 2020; Schill et al., 2020; Zuidema et al., 2018) this work also indicates a need for greater consideration of the impacts of smoke in the MBL, especially during the boreal winter. Previous research conducted at Ragged Point has primarily focused on African dust, which reaches its maximum during the boreal summer when smoke transport is low (Zuidema et al., 2019). To better contextualize our findings, we analysed carbon monoxide column density (a tracer for smoke) as well as aerosol optical depth (AOD;~~) and aerosol optical thickness (AOT)~~ ~~(~~a tracer~~s~~ for dust and smoke) from 2018-2022 (Figure S4 and S5). Figure S4 shows the temporal trends while Figure S5 show seasonal averages. As expected, AOD~~ and AOT~~ peaks in July when dust transport reaches a maximum. However, Figures S4 and S5 indicate that smoke is decoupled from dust, reaching a maximum in the spring around April and a minimum in the summer when dust transport is highest. This finding suggests that while the dust transport during the EUREC4A/ATOMIC campaigns is higher than average dust loadings during this month (Zuidema et al., 2019), the amount of smoke observed is not unique, but rather characteristic of the region. This is consistent with observations in Amazonia, where smoke and dust transport during boreal winter and spring has been found consistently since the first measurement campaign in 1987 (Talbot et al., 1990; Andreae et al., 2015; Moran-Zuloaga et al., 2018) . Further, wintertime aerosol transport is typically transported at lower altitudes as the height of emission for wintertime aerosols is lower compared to summertime aerosol transport, leading to greater mixing into the MBL (Gutleben et al., 2022; Tsamalis et al., 2013). Thus, smoke may be playing an important role on CCN formation throughout a large portion of the year. This is especially true considering the large size of long-range transported smoke plumes that have a wide geographic extent in which they can affect cloud formation. To conclude, this work highlights the need to characterize African smoke transport to Ragged Point and better understand the role of smoke in cloud formation, radiative forcing, and climate (Pechony & Shindell, 2010; Shindell et al., 2009).

Data Availability

The data will be made publically available in the University of Miami data repository and will be linked with a doi.

Author Contributions

Conceptualization of this work was done by HMR, MLP, OK, and CJG. Collection of samples was conducted by HMR, OK, EB, and PS, while analysis was done by HMR, MLP, OK, NNL, and ZC. The development of the methods used in this work was done by HMR, MLP, OK, ZC, SC, APA, and CJG. Instrumentation used to conduct this work were provided by MLP, SC, APA, and CJG. Formal analysis of data was performed by HMR, MLP, CP, and OK. Validation of data products was performed by HMR, ZC, SC, APA, and CJG. Computer code used for data analysis was provided by MLP, OK, and APA. Data visualization was performed by HMR, MLP, and OK. PKQ, PZ, CP, and UP helped interpret results. Supervision and project administration duties were done by MLP and CJG. HMR wrote the original draft for publication, and all co-authors reviewed and edited this work.

Competing Interests

Some authors are members of the editorial board of Atmospheric Chemistry and Physics. The peer-review process was guided by an independent editor, and the authors have no other competing interests to declare

Acknowledgements

C.J.G. acknowledges an NSF CAREER award (1944958). A portion of this research was performed on project awards (10.46936/lser.proj.2019.50816/60000110 and 10.46936/lser.proj.2021.51900/60000361) from the Environmental Molecular Sciences Laboratory, a DOE Office of Science User Facility sponsored by the Biological and Environmental Research program under Contract No. DE-AC05-76RL01830. P.K.Q. acknowledges PMEL contribution number 5353. MLP and CP acknowledge support by the Max Planck Society. P.Z. acknowledges support from the NOAA grant OAR CPO NA19OAR4310379.

References

Abel, S. J., Haywood, J. M., Highwood, E. J., Li, J., & Buseck, P. R. (2003). Evolution of biomass burning aerosol properties from an agricultural fire in southern Africa. *Geophysical Research Letters*, *30*(15). https://doi.org/https://doi.org/10.1029/2003GL017342

Adams, A. M., Prospero, J. M., & Zhang, C. (2012). CALIPSO-Derived Three-Dimensional Structure of Aerosol over the Atlantic Basin and Adjacent Continents. *Journal of Climate*, *25*, 6862–6879.

Albrecht, B. A. (1989). Aerosols, cloud microphysics, and fractional cloudiness. *Science*, *245*(4923), 1227–1230. https://doi.org/10.1126/science.245.4923.1227

Allan, J. D., Baumgardner, D., Raga, G. B., Mayol-Bracero, O. L., Morales-García, F., García-García, F., Montero-Martínez, G., Borrmann, S., Schneider, J., Mertes, S., Walter, S., Gysel, M., Dusek, U., Frank, G. P., & Krämer, M. (2008). Clouds and aerosols in Puerto Rico – a new evaluation. *Atmospheric Chemistry and Physics*, *8*(5), 1293–1309. https://doi.org/10.5194/acp-8-1293-2008

Andreae, M. O. (1983). Soot Carbon and Excess Fine Potassium: Long-Range Transport of Combustion-Derived Aerosols. *Science*, *220*(4602), 1148–1151. https://doi.org/10.1126/science.220.4602.1148

Andreae, M. O. (2019). Emission of trace gases and aerosols from biomass burning -- an updated assessment. *Atmospheric Chemistry and Physics*, *19*(13), 8523–8546. https://doi.org/10.5194/acp-19-8523-2019

Ansmann, A., Baars, H., Tesche, M., Müller, D., Althausen, D., Engelmann, R., Pauliquevis, T., & Artaxo, P. (2009). Dust and smoke transport from Africa to South America: Lidar profiling over Cape Verde and the Amazon rainforest. *Geophysical Research Letters*, *36*(11). https://doi.org/https://doi.org/10.1029/2009GL037923

Archibald, A. T., Witham, C. S., Ashfold, M. J., Manning, A. J., O'Doherty, S., Greally, B. R., Young, D., & Shallcross, D. E. (2015). Long-term high frequency measurements of ethane, benzene and methyl chloride at Ragged Point, Barbados: Identification of long-range transport events. *Elementa: Science of the Anthropocene*, *3*. https://doi.org/10.12952/journal.elementa.000068

Asa-Awuku, A., Sullivan, A. P., Hennigan, C. J., Weber, R. J., & Nenes, A. (2008). Investigation of molar volume and surfactant characteristics of water-soluble organic compounds in biomass burning aerosol. *Atmos. Chem. Phys.*, *8*(4), 799–812. https://doi.org/10.5194/acp-8-799-2008

Ault, A. P., Guasco, T. L., Baltrusaitis, J., Ryder, O. S., Trueblood, J. v, Collins, D. B., Ruppel, M. J., Cuadra-Rodriguez, L. A., Prather, K. A., & Grassian, V. H. (2014). Heterogeneous Reactivity of Nitric Acid with Nascent Sea Spray Aerosol: Large Differences Observed between and within Individual Particles. *The Journal of Physical Chemistry Letters*, *5*(15), 2493–2500. https://doi.org/10.1021/jz5008802

Ault, A. P., Guasco, T. L., Ryder, O. S., Baltrusaitis, J., Cuadra-Rodriguez, L. A., Collins, D. B., Ruppel, M. J., Bertram, T. H., Prather, K. A., & Grassian, V. H. (2013). Inside versus outside: Ion redistribution in nitric acid reacted sea spray aerosol particles as determined by single particle analysis. *Journal of the American Chemical Society*, *135*(39), 14528–14531. https://doi.org/10.1021/ja407117x

Ault, A. P., Moffet, R. C., Baltrusaitis, J., Collins, D. B., Ruppel, M. J., Cuadra-Rodriguez, L. A., Zhao, D., Guasco, T. L., Ebben, C. J., Geiger, F. M., Bertram, T. H., Prather, K. A., & Grassian, V. H. (2013). Size-Dependent Changes in Sea Spray Aerosol Composition and Properties with Different Seawater Conditions. *Environmental Science & Technology*, *47*(11), 5603–5612. https://doi.org/10.1021/es400416g

Ault, A. P., Peters, T. M., Sawvel, E. J., Casuccio, G. S., Willis, R. D., Norris, G. A., & Grassian, V. H. (2012). Single-Particle SEM-EDX Analysis of Iron-Containing Coarse Particulate Matter in an Urban Environment: Sources and Distribution of Iron within Cleveland, Ohio. *Environmental Science & Technology*, *46*(8), 4331–4339. https://doi.org/10.1021/es204006k

Ault, A. P., Zhao, D., Ebben, C. J., Tauber, M. J., Geiger, F. M., Prather, K. A., & Grassian, V. H. (2013). Raman microspectroscopy and vibrational sum frequency generation spectroscopy as probes of the bulk and surface compositions of size-resolved sea spray aerosol particles. *Physical Chemistry Chemical Physics*, *15*(17), 6206–6214. https://doi.org/10.1039/C3CP43899F

Barkley, A. E., Olson, N. E., Prospero, J. M., Gatineau, A., Panechou, K., Maynard, N. G., Blackwelder, P., China, S., Ault, A. P., & Gaston, C. J. (2021). Atmospheric Transport of North African Dust-Bearing Supermicron Freshwater Diatoms to South America: Implications for Iron Transport to the Equatorial North Atlantic Ocean. *Geophysical Research Letters*, *48*(5), e2020GL090476. https://doi.org/https://doi.org/10.1029/2020GL090476

Barkley, A. E., Prospero, J. M., Mahowald, N., Hamilton, D. S., Popendorf, K. J., Oehlert, A. M., Pourmand, A., Gatineau, A., Panechou-Pulcherie, K., Blackwelder, P., & Gaston, C. J. (2019). African biomass burning is a substantial source of phosphorus deposition to the Amazon, Tropical Atlantic Ocean, and Southern Ocean. *Proceedings of the National Academy of Sciences*, *116*(33), 16216 LP – 16221. https://doi.org/10.1073/pnas.1906091116

Bates, T. S., Lamb, B. K., Guenther, A., Dignon, J., & Stoiber, R. E. (1992). Sulfur emissions to the atmosphere from natural sourees. *Journal of Atmospheric Chemistry*, *14*(1), 315–337. https://doi.org/10.1007/BF00115242

Behnke, W., George, C., Scheer, V., & Zetzsch, C. (1997). Production and decay of ClNO2 from the reaction of gaseous N2O5 with NaCl solution: Bulk and aerosol experiments. *Journal of Geophysical Research Atmospheres*, *102*(3), 3795–3804. https://doi.org/10.1029/96jd03057

Behrenfeld, M. J., Moore, R. H., Hostetler, C. A., Graff, J., Gaube, P., Russell, L. M., Chen, G., Doney, S. C., Giovannoni, S., Liu, H., Proctor, C., Bolaños, L. M., Baetge, N., Davie-Martin, C., Westberry, T. K., Bates, T. S., Bell, T. G., Bidle, K. D., Boss, E. S., … Ziemba, L. (2019). The North Atlantic Aerosol and Marine Ecosystem Study (NAAMES): Science Motive and Mission Overview . In *Frontiers in Marine Science* (Vol. 6). https://www.frontiersin.org/article/10.3389/fmars.2019.00122

Bondy, A. L., Bonanno, D., Moffet, R. C., Wang, B., Laskin, A., & Ault, A. P. (2018). The diverse chemical mixing state of aerosol particles in the southeastern United States. *Atmospheric Chemistry and Physics*, *18*(16), 12595–12612. https://doi.org/10.5194/acp-18-12595-2018

Capes, G., Johnson, B., McFiggans, G., Williams, P. ~I., Haywood, J., & Coe, H. (2008). Aging of biomass burning aerosols over West Africa: Aircraft measurements of chemical composition, microphysical properties, and emission ratios. *Journal of Geophysical Research (Atmospheres)*, *113*(D23), D00C15. https://doi.org/10.1029/2008JD009845

Cappa, C. D., Lim, C. Y., Hagan, D. H., Coggon, M., Koss, A., Sekimoto, K., de Gouw, J., Onasch, T. B., Warneke, C., & Kroll, J. H. (2020). Biomass-burning-derived particles from a wide variety of fuels -- Part 2: Effects of photochemical aging on particle optical and chemical properties. *Atmospheric Chemistry and Physics*, *20*(14), 8511–8532. https://doi.org/10.5194/acp-20-8511-2020

Carlson, T. N., & Prospero, J. M. (1972). The Large-Scale Movement of Saharan Air Outbreaks over the Northern Equatorial Atlantic. *Journal of Applied Meteorology and Climatology*, *11*(2), 283–297. https://doi.org/10.1175/1520-0450(1972)011<0283:TLSMOS>2.0.CO;2

Carslaw, K. S., Lee, L. A., Reddington, C. L., Pringle, K. J., Rap, A., Forster, P. M., Mann, G. W., Spracklen, D. v, Woodhouse, M. T., Regayre, L. A., & Pierce, J. R. (2013). Large contribution of natural aerosols to uncertainty in indirect forcing. *Nature*, *503*(7474), 67–71. https://doi.org/10.1038/nature12674

Chin, M., Diehl, T., Tan, Q., Prospero, J. M., Kahn, R. A., Remer, L. A., Yu, H., Sayer, A. M., Bian, H., Geogdzhayev, I. v, Holben, B. N., Howell, S. G., Huebert, B. J., Hsu, N. C., Kim, D., Kucsera, T. L., Levy, R. C., Mishchenko, M. I., Pan, X., … Zhao, X.-P. (2014). Multi-decadal aerosol variations from 1980 to 2009: a perspective from observations and a global model. *Atmospheric Chemistry and Physics*, *14*(7), 3657–3690. https://doi.org/10.5194/acp-14-3657-2014

Choël, M., Deboudt, K., Flament, P., Aimoz, L., & Mériaux, X. (2007). Single-particle analysis of atmospheric aerosols at Cape Gris-Nez, English Channel: Influence of steel works on iron apportionment. *Atmospheric Environment*, *41*(13), 2820–2830. https://doi.org/https://doi.org/10.1016/j.atmosenv.2006.11.038

Dang, C., Segal-Rozenhaimer, M., Che, H., Zhang, L., Formenti, P., Taylor, J., Dobracki, A., Purdue, S., Wong, P.-S., Nenes, A., Sedlacek, A., Coe, H., Redemann, J., Zuidema, P., & Haywood, J. (2021). Biomass burning and marine aerosol processing over the southeast Atlantic Ocean: A TEM single particle analysis. *Atmos. Chem. Phys. Discuss.*, *2021*, 1–30. https://doi.org/10.5194/acp-2021-724

Dang, C., Segal-Rozenhaimer, M., Che, H., Zhang, L., Formenti, P., Taylor, J., Dobracki, A., Purdue, S., Wong, P.-S., Nenes, A., Sedlacek III, A., Coe, H., Redemann, J., Zuidema, P., Howell, S., & Haywood, J. (2022). Biomass burning and marine aerosol processing over the southeast Atlantic Ocean: a TEM single-particle analysis. *Atmospheric Chemistry and Physics*, *22*(14), 9389–9412. https://doi.org/10.5194/acp-22-9389-2022

Deboudt, K., Flament, P., Choël, M., Gloter, A., Sobanska, S., & Colliex, C. (2010). Mixing state of aerosols and direct observation of carbonaceous and marine coatings on African dust by individual particle analysis. *Journal of Geophysical Research: Atmospheres*, *115*(D24). https://doi.org/https://doi.org/10.1029/2010JD013921

Denjean, C., Caquineau, S., Desboeufs, K., Laurent, B., Maille, M., Quiñones Rosado, M., Vallejo, P., Mayol-Bracero, O. L., & Formenti, P. (2015). Long-range transport across the Atlantic in summertime does not enhance the hygroscopicity of African mineral dust. *Geophysical Research Letters*, *42*(18), 7835–7843. https://doi.org/https://doi.org/10.1002/2015GL065693

Dusek, U., Frank, G. P., Hildebrandt, L., Curtius, J., Schneider, J., Walter, S., Chand, D., Drewnick, F., Hings, S., Jung, D., Borrmann, S., & Andreae, M. O. (2006). Size Matters More Than Chemistry for Cloud-Nucleating Ability of Aerosol Particles. *Science*, *312*(5778), 1375–1378. https://doi.org/10.1126/science.1125261

Echalar, F., Gaudichet, A., Cachier, H., & Artaxo, P. (1995). Aerosol emissions by tropical forest and savanna biomass burning: Characteristic trace elements and fluxes. *Geophysical Research Letters*, *22*(22), 3039–3042. https://doi.org/https://doi.org/10.1029/95GL03170

Edwards, E.-L., Corral, A. F., Dadashazar, H., Barkley, A. E., Gaston, C. J., Zuidema, P., & Sorooshian, A. (2021). Impact of various air mass types on cloud condensation nuclei concentrations along coastal southeast Florida. *Atmospheric Environment*, *254*, 118371. https://doi.org/https://doi.org/10.1016/j.atmosenv.2021.118371

Engelhart, G. J., Hennigan, C. J., Miracolo, M. A., Robinson, A. L., & Pandis, S. N. (2012). Cloud condensation nuclei activity of fresh primary and aged biomass burning aerosol. *Atmospheric Chemistry and Physics*, *12*(15), 7285–7293. https://doi.org/10.5194/acp-12-7285-2012

Facchini, M. C., Mircea, M., Fuzzi, S., & Charlson, R. J. (1999). Cloud albedo enhancement by surface-active organic solutes in growing droplets. *Nature*, *401*(6750), 257–259. https://doi.org/10.1038/45758

Forster, P., Storelvmo, T., Armour, K., William, C., Dufresne, J.-L., Frame, D., Lunt, D., Mauritsen, T., Palmer, M., Watanabe, M., Wild, M., & Zhang, H. (2021). Chapter 7: The Earth's energy budget, climate feedbacks, and climate sensitivity. *Climate Change 2021: The Physical Science Basis, Contributi*.

Freney, E. J., Martin, S. T., & Buseck, P. R. (2009). Deliquescence and efflorescence of potassium salts relevant to biomass-burning aerosol particles. *Aerosol Science and Technology*, *43*(8), 799–807. https://doi.org/10.1080/02786820902946620

Gaston, C. J., Furutani, H., Guazzotti, S. A., Coffee, K. R., Bates, T. S., Quinn, P. K., Aluwihare, L. I., Mitchell, B. G., & Prather, K. A. (2011). Unique ocean-derived particles serve as a proxy for changes in ocean chemistry. *Journal of Geophysical Research Atmospheres*, *116*(18), 1–13. https://doi.org/10.1029/2010JD015289

Gaston, C. J., Pratt, K. A., Qin, X., & Prather, K. A. (2010). Real-time detection and mixing state of methanesulfonate in single particles at an inland urban location during a phytoplankton bloom. *Environmental Science and Technology*, *44*(5), 1566–1572. https://doi.org/10.1021/es902069d

Gaston, C. J., Quinn, P. K., Bates, T. S., Gilman, J. B., Bon, D. M., Kuster, W. C., & Prather, K. A. (2013). The impact of shipping, agricultural, and urban emissions on single particle chemistry observed aboard the R/V Atlantis during CalNex. *Journal of Geophysical Research Atmospheres*, *118*(10), 5003–5017. https://doi.org/10.1002/jgrd.50427

Gérard, V., Nozière, B., Baduel, C., Fine, L., Frossard, A. A., & Cohen, R. C. (2016). Anionic, Cationic, and Nonionic Surfactants in Atmospheric Aerosols from the Baltic Coast at Askö, Sweden: Implications for Cloud Droplet Activation. *Environmental Science & Technology*, *50*(6), 2974–2982. https://doi.org/10.1021/acs.est.5b05809

Giordano, M., Espinoza, C., & Asa-Awuku, A. (2015). Experimentally measured morphology of biomass burning aerosol and its impacts on CCN ability. *Atmospheric Chemistry and Physics*, *15*(4), 1807–1821. https://doi.org/10.5194/acp-15-1807-2015

Good, N., Topping, D. O., Allan, J. D., Flynn, M., Fuentes, E., Irwin, M., Williams, P. I., Coe, H., & McFiggans, G. (2010). Consistency between parameterisations of aerosol hygroscopicity and CCN activity during the RHaMBLe discovery cruise. *Atmos. Chem. Phys.*, *10*(7), 3189–3203. https://doi.org/10.5194/acp-10-3189-2010

Gutleben, M., Groß, S., Heske, C., & Wirth, M. (2022). Wintertime Saharan dust transport towards the Caribbean: an airborne lidar case study during EUREC^{4}A. *Atmospheric Chemistry and Physics*, *22*(11), 7319–7330. https://doi.org/10.5194/acp-22-7319-2022

Hand, V. L., Capes, G., Vaughan, D. J., Formenti, P., Haywood, J. M., & Coe, H. (2010). Evidence of internal mixing of African dust and biomass burning particles by individual particle analysis using electron beam techniques. *Journal of Geophysical Research: Atmospheres*, *115*(D13). https://doi.org/https://doi.org/10.1029/2009JD012938

Hennigan, C. J., Miracolo, M. A., Engelhart, G. J., May, A. A., Presto, A. A., Lee, T., Sullivan, A. P., McMeeking, G. R., Coe, H., Wold, C. E., Hao, W.-M., Gilman, J. B., Kuster, W. C., de Gouw, J., Schichtel, B. A., Collett Jr., J. L., Kreidenweis, S. M., & Robinson, A. L. (2011). Chemical and physical transformations of organic aerosol from the photo-oxidation of open biomass burning emissions in an environmental chamber. *Atmospheric Chemistry and Physics*, *11*(15), 7669–7686. https://doi.org/10.5194/acp-11-7669-2011

Hennigan, C. J., Sullivan, A. P., Collett Jr., J. L., & Robinson, A. L. (2010). Levoglucosan stability in biomass burning particles exposed to hydroxyl radicals. *Geophysical Research Letters*, *37*(9). https://doi.org/https://doi.org/10.1029/2010GL043088

Hodshire, A. L., Akherati, A., Alvarado, M. J., Brown-Steiner, B., Jathar, S. H., Jimenez, J. L., Kreidenweis, S. M., Lonsdale, C. R., Onasch, T. B., Ortega, A. M., & Pierce, J. R. (2019). Aging Effects on Biomass Burning Aerosol Mass and Composition: A Critical Review of Field and Laboratory Studies. *Environmental Science & Technology*, *53*(17), 10007–10022. https://doi.org/10.1021/acs.est.9b02588

Hoffman, R. C., Laskin, A., & Finlayson-Pitts, B. J. (2004). Sodium nitrate particles: physical and chemical properties during hydration and dehydration, and implications for aged sea salt aerosols. *Journal of Aerosol Science*, *35*(7), 869–887. https://doi.org/https://doi.org/10.1016/j.jaerosci.2004.02.003

Holanda, B. A., Pöhlker, M. L., Walter, D., Saturno, J., Sörgel, M., Ditas, J., Ditas, F., Schulz, C., Franco, M. A., Wang, Q., Donth, T., Artaxo, P., Barbosa, H. M. J., Borrmann, S., Braga, R., Brito, J., Cheng, Y., Dollner, M., Kaiser, J. W., … Pöhlker, C. (2020). Influx of African biomass burning aerosol during the Amazonian dry season through layered transatlantic transport of black carbon-rich smoke. *Atmospheric Chemistry and Physics*, *20*(8), 4757–4785. https://doi.org/10.5194/acp-20-4757-2020

Hoppel, W. A., Frick, G. M., & Larson, R. E. (1986). Effect of nonprecipitating clouds on the aerosol size distribution in the marine boundary layer. *Geophysical Research Letters*, *13*(2), 125–128. https://doi.org/https://doi.org/10.1029/GL013i002p00125

Hudson, P. K., Murphy, D. M., Cziczo, D. J., Thomson, D. S., de Gouw, J. A., Warneke, C., Holloway, J., Jost, H.-J., & Hübler, G. (2004). Biomass-burning particle measurements: Characteristic composition and chemical processing. *Journal of Geophysical Research: Atmospheres*, *109*(D23). https://doi.org/https://doi.org/10.1029/2003JD004398

Jimenez, J. L., Canagaratna, M. R., Donahue, N. M., Prevot, A. S. H., Zhang, Q., Kroll, J. H., DeCarlo, P. F., Allan, J. D., Coe, H., Ng, N. L., Aiken, A. C., Docherty, K. S., Ulbrich, I. M., Grieshop, A. P., Robinson, A. L., Duplissy, J., Smith, J. D., Wilson, K. R., Lanz, V. A., … Worsnop, D. R. (2009). Evolution of organic aerosols in the atmosphere. *Science*, *326*(5959), 1525–1529. https://doi.org/10.1126/science.1180353

Kacarab, M., Thornhill, K. L., Dobracki, A., Howell, S. G., O'Brien, J. R., Freitag, S., Poellot, M. R., Wood, R., Zuidema, P., Redemann, J., & Nenes, A. (2020). Biomass burning aerosol as a modulator of the droplet number in the southeast Atlantic region. *Atmos. Chem. Phys.*, *20*(5), 3029–3040. https://doi.org/10.5194/acp-20-3029-2020

Kitto, M. E., & Anderson, D. L. (1988). The use of Whatman-41 filters for particle. *Atmospheric Environment (1967)*, *22*(11), 2629–2630. https://doi.org/https://doi.org/10.1016/0004-6981(88)90500-8

Klingebiel, M., Ghate, V. P., Naumann, A. K., Ditas, F., Pöhlker, M. L., Pöhlker, C., Kandler, K., Konow, H., & Stevens, B. (2019). Remote Sensing of Sea Salt Aerosol below Trade Wind Clouds. *Journal of the Atmospheric Sciences*, *76*(5), 1189–1202. https://doi.org/10.1175/JAS-D-18-0139.1

Konovalov, I. B., Golovushkin, N. A., Beekmann, M., & Andreae, M. O. (2021). Insights into the aging of biomass burning aerosol from satellite observations and 3D atmospheric modeling: evolution of the aerosol optical properties in Siberian wildfire plumes. *Atmospheric Chemistry and Physics*, *21*(1), 357–392. https://doi.org/10.5194/acp-21-357-2021

Kristensen, T. B., Müller, T., Kandler, K., Benker, N., Hartmann, M., Prospero, J. M., Wiedensohler, A., & Stratmann, F. (2016). Properties of cloud condensation nuclei (CCN) in the trade wind marine boundary layer of the western North Atlantic. *Atmos. Chem. Phys.*, *16*(4), 2675–2688. https://doi.org/10.5194/acp-16-2675-2016

Krueger, B. J., Grassian, V. H., Cowin, J. P., & Laskin, A. (2004). Heterogeneous chemistry of individual mineral dust particles from different dust source regions: the importance of particle mineralogy. *Atmospheric Environment*, *38*(36), 6253–6261. https://doi.org/https://doi.org/10.1016/j.atmosenv.2004.07.010

Laskin, A., Moffet, R. C., Gilles, M. K., Fast, J. D., Zaveri, R. A., Wang, B., Nigge, P., & Shutthanandan, J. (2012). Tropospheric chemistry of internally mixed sea salt and organic particles: Surprising reactivity of NaCl with weak organic acids. *Journal of Geophysical Research: Atmospheres*, *117*(D15). https://doi.org/https://doi.org/10.1029/2012JD017743

Laskin, A., Wietsma, T. W., Krueger, B. J., & Grassian, V. H. (2005). Heterogeneous chemistry of individual mineral dust particles with nitric acid: A combined CCSEM/EDX, ESEM, and ICP-MS study. *Journal of Geophysical Research: Atmospheres*, *110*(D10). https://doi.org/https://doi.org/10.1029/2004JD005206

Lathem, T. L., Beyersdorf, A. J., Thornhill, K. L., Winstead, E. L., Cubison, M. J., Hecobian, A., Jimenez, J. L., Weber, R. J., Anderson, B. E., & Nenes, A. (2013). Analysis of CCN activity of Arctic aerosol and Canadian biomass burning during summer 2008. *Atmospheric Chemistry and Physics*, *13*(5), 2735–2756. https://doi.org/10.5194/acp-13-2735-2013

Levin, Z., Teller, A., Ganor, E., & Yin, Y. (2005). On the interactions of mineral dust, sea-salt particles, and clouds: A measurement and modeling study from the Mediterranean Israeli Dust Experiment campaign. *Journal of Geophysical Research: Atmospheres*, *110*(D20). https://doi.org/https://doi.org/10.1029/2005JD005810

Li, J., Pósfai, M., Hobbs, P. v, & Buseck, P. R. (2003). Individual aerosol particles from biomass burning in southern Africa: 2, Compositions and aging of inorganic particles. *Journal of Geophysical Research: Atmospheres*, *108*(D13). https://doi.org/https://doi.org/10.1029/2002JD002310

Li, W., Shao, L., Wang, Z., Shen, R., Yang, S., & Tang, U. (2010). Size, composition, and mixing state of individual aerosol particles in a South China coastal city. *Journal of Environmental Sciences*, *22*(4), 561–569. https://doi.org/https://doi.org/10.1016/S1001-0742(09)60146-7

Maenhaut, W., Salma, I., Cafmeyer, J., Annegarn, H. J., & Andreae, M. O. (1996). Regional atmospheric aerosol composition and sources in the eastern Transvaal, South Africa, and impact of biomass burning. *Journal of Geophysical Research: Atmospheres*, *101*(D19), 23631–23650. https://doi.org/https://doi.org/10.1029/95JD02930

Massoli, P., Lambe, A. T., Ahern, A. T., Williams, L. R., Ehn, M., Mikkilä, J., Canagaratna, M. R., Brune, W. H., Onasch, T. B., Jayne, J. T., Petäjä, T., Kulmala, M., Laaksonen, A., Kolb, C. E., Davidovits, P., & Worsnop, D. R. (2010). Relationship between aerosol oxidation level and hygroscopic properties of laboratory generated secondary organic aerosol (SOA) particles. *Geophysical Research Letters*, *37*(24). https://doi.org/https://doi.org/10.1029/2010GL045258

McCoy, D. T., Burrows, S. M., Wood, R., Grosvenor, D. P., Elliott, S. M., Ma, P.-L., Rasch, P. J., & Hartment, D. L. (2022). Natural aerosols explain seasonal and spatial patterns of Southern Ocean cloud albedo. *Science Advances*, *1*(6), e1500157. https://doi.org/10.1126/sciadv.1500157

McFiggans, G., Artaxo, P., Baltensperger, U., Coe, H., Facchini, M. C., Feingold, G., Fuzzi, S., Gysel, M., Laaksonen, A., Lohmann, U., Mentel, T. F., Murphy, D. M., O'Dowd, C. D., Snider, J. R., & Weingartner, E. (2006). The effect of physical and chemical aerosol properties on warm cloud droplet activation. *Atmospheric Chemistry and Physics*, *6*(9), 2593–2649. https://doi.org/10.5194/acp-6-2593-2006

Miles, J. C., Crutzen, P. J., & Goldammer, J. G. (1995). Fire in the Environment: The Ecological, Atmospheric and Climatic Importance of Vegetation Fires. *Journal of Ecology*, *83*, 549.

Miller, R. M., McFarquhar, G. M., Rauber, R. M., O'Brien, J. R., Gupta, S., Segal-Rozenhaimer, M., Dobracki, A. N., Sedlacek, A. J., Burton, S. P., Howell, S. G., Freitag, S., & Dang, C. (2021). Observations of supermicron-sized aerosols originating from biomass burning in southern Central Africa. *Atmos. Chem. Phys.*, *21*(19), 14815–14831. https://doi.org/10.5194/acp-21-14815-2021

Moran-Zuloaga, D., Ditas, F., Walter, D., Saturno, J., Brito, J., Carbone, S., Chi, X., de Angelis, I., Baars, H., Godoi, R. H. M., Heese, B., Holanda, B. A., Lavrič, J. v, Martin, S. T., Ming, J., Pöhlker, M. L., Ruckteschler, N., Su, H., Wang, Y., … Pöhlker, C. (2018). Long-term study on coarse mode aerosols in the Amazon rain forest with the frequent intrusion of Saharan dust plumes. *Atmospheric Chemistry and Physics*, *18*(13), 10055–10088. https://doi.org/10.5194/acp-18-10055-2018

Murphy, D. M., Cziczo, D. J., Froyd, K. D., Hudson, P. K., Matthew, B. M., Middlebrook, A. M., Peltier, R. E., Sullivan, A., Thomson, D. S., & Weber, R. J. (2006). Single-particle mass spectrometry of tropospheric aerosol particles. *Journal of Geophysical Research: Atmospheres*, *111*(D23). https://doi.org/https://doi.org/10.1029/2006JD007340

Nájera, J. J., & Horn, A. B. (2009). Infrared spectroscopic study of the effect of oleic acid on the deliquescence behaviour of ammonium sulfate aerosol particles. *Physical Chemistry Chemical Physics*, *11*(3), 483–494. https://doi.org/10.1039/B812182F

O'Dowd, C. D., & de Leeuw, G. (2007). Marine aerosol production: a review of the current knowledge. *Philosophical Transactions of the Royal Society A: Mathematical, Physical and Engineering Sciences*, *365*(1856), 1753–1774. https://doi.org/10.1098/rsta.2007.2043

O'Dowd, C. D., Facchini, M. C., Cavalli, F., Ceburnis, D., Mircea, M., Decesari, S., Fuzzi, S., Yoon, Y. J., & Putaud, J.-P. (2004). Biogenically driven organic contribution to marine aerosol. *Nature*, *431*(7009), 676–680. https://doi.org/10.1038/nature02959

Ovadnevaite, J., Zuend, A., Laaksonen, A., Sanchez, K. J., Roberts, G., Ceburnis, D., Decesari, S., Rinaldi, M., Hodas, N., Facchini, M. C., Seinfeld, J. H., & O' Dowd, C. (2017). Surface tension prevails over solute effect in organic-influenced cloud droplet activation. *Nature*, *546*(7660), 637–641. https://doi.org/10.1038/nature22806

Pachauri, T., Singla, V., Satsangi, A., Lakhani Anita, & Kumari, K. M. (2013). SEM-EDX Characterization of Individual Coarse Particles in Agra, India. *Aerosol and Air Quality Research*, *13*(2), 523–536. https://doi.org/10.4209/aaqr.2012.04.0095

Petters, M. D., & Kreidenweis, S. M. (2007). A single parameter representation of hygroscopic growth and cloud condensation nucleus activity. *Atmospheric Chemistry and Physics*, *7*(8), 1961–1971. https://doi.org/10.5194/acp-7-1961-2007

Pierce, J. R., Chen, K., & Adams, P. J. (2007). Contribution of primary carbonaceous aerosol to cloud condensation nuclei: processes and uncertainties evaluated with a global aerosol microphysics model. *Atmospheric Chemistry and Physics*, *7*(20), 5447–5466. https://doi.org/10.5194/acp-7-5447-2007

Pöhlker, M. L., Pöhlker, C., Ditas, F., Klimach, T., de Angelis, I., Araújo, A., Brito, J., Carbone, S., Cheng, Y., Chi, X., Ditz, R., Gunthe, S. S., Kesselmeier, J., Könemann, T., Lavrič, J. v, Martin, S. T., Mikhailov, E., Moran-Zuloaga, D., Rose, D., … Pöschl, U. (2016). Long-term observations of cloud condensation nuclei in the Amazon rain forest -- Part 1: Aerosol size distribution, hygroscopicity, and new model parametrizations for CCN prediction. *Atmospheric Chemistry and Physics*, *16*(24), 15709–15740. https://doi.org/10.5194/acp-16-15709-2016

Pósfai, M., Simonics, R., Li, J., Hobbs, P. v, & Buseck, P. R. (2003). Individual aerosol particles from biomass burning in southern Africa: 1. Compositions and size distributions of carbonaceous particles. *Journal of Geophysical Research: Atmospheres*, *108*(D13). https://doi.org/https://doi.org/10.1029/2002JD002291

Prisle, N. L., Raatikainen, T., Laaksonen, A., & Bilde, M. (2010). Surfactants in cloud droplet activation: mixed organic-inorganic particles. *Atmospheric Chemistry and Physics*, *10*(12), 5663–5683. https://doi.org/10.5194/acp-10-5663-2010

Prospero, J. M. (1968). atmospheric dust studies on Barbados. *Bulletin of the American Meteorological Society*, *49*(6), 645–652. https://doi.org/10.1175/1520-0477-49.6.645

Prospero, J. M. (1999). Long-range transport of mineral dust in the global atmosphere: Impact of African dust on the environment of the southeastern United States. *Proceedings of the National Academy of Sciences*, *96*(7), 3396 LP – 3403. https://doi.org/10.1073/pnas.96.7.3396

Prospero, J. M., Barkley, A. E., Gaston, C. J., Gatineau, A., Campos y Sansano, A., & Panechou, K. (2020). Characterizing and Quantifying African Dust Transport and Deposition to South America: Implications for the Phosphorus Budget in the Amazon Basin. *Global Biogeochemical Cycles*, *34*(9), e2020GB006536. https://doi.org/https://doi.org/10.1029/2020GB006536

Prospero, J. M., Blades, E., Mathison, G., & Naidu, R. (2005). Interhemispheric transport of viable fungi and bacteria from Africa to the Caribbean with soil dust. *Aerobiologia*, *21*(1), 1–19. https://doi.org/10.1007/s10453-004-5872-7

Prospero, J. M., Collard, F.-X., Molinié, J., & Jeannot, A. (2014). Characterizing the annual cycle of African dust transport to the Caribbean Basin and South America and its impact on the environment and air quality. *Global Biogeochemical Cycles*, *28*(7), 757–773. https://doi.org/https://doi.org/10.1002/2013GB004802

Prospero, J. M., Delany, A. C., Delany, A. C., & Carlson, T. N. (2021). The Discovery of African Dust Transport to the Western Hemisphere and the Saharan Air Layer: A History. *Bulletin of the American Meteorological Society*, *102*(6), E1239–E1260. https://doi.org/10.1175/BAMS-D-19-0309.1

Prospero, J. M., Glaccum, R. A., & Nees, R. T. (1981). Atmospheric transport of soil dust from Africa to South America. *Nature*, *289*(5798), 570–572. https://doi.org/10.1038/289570a0

Prospero, J. M., & Lamb, P. J. (n.d.). *prospero2003*.

Prospero, J. M., & Lamb, P. J. (2003). African Droughts and Dust Transport to the Caribbean: Climate Change Implications. *Science*, *302*(5647), 1024–1027. https://doi.org/10.1126/science.1089915

Prospero, J. M., & Mayol-Bracero, O. L. (2013). Understanding the Transport and Impact of African Dust on the Caribbean Basin. *Bulletin of the American Meteorological Society*, *94*(9), 1329–1337. https://doi.org/10.1175/BAMS-D-12-00142.1

Pszenny, A., Fischer, C., Mendez, A., & Zetwo, M. (1993). Direct comparison of cellulose and quartz fiber filters for sampling submicrometer aerosols in the marine boundary layer. *Atmospheric Environment. Part A. General Topics*, *27*(2), 281–284. https://doi.org/https://doi.org/10.1016/0960-1686(93)90359-7

Quinn, P. K., Bates, T. S., Coffman, D. J., & Covert, D. S. (2008). Influence of particle size and chemistry on the cloud nucleating properties of aerosols. *Atmospheric Chemistry and Physics*, *8*(4), 1029–1042. https://doi.org/10.5194/acp-8-1029-2008

Quinn, P. K., Thompson, E. J., Coffman, D. J., Baidar, S., Bariteau, L., Bates, T. S., Bigorre, S., Brewer, A., de Boer, G., de Szoeke, S. P., Drushka, K., Foltz, G. R., Intrieri, J., Iyer, S., Fairall, C. W., Gaston, C. J., Jansen, F., Johnson, J. E., Krüger, O. O., … Zuidema, P. (2021). Measurements from the RV Ronald

H. Brown and related platforms as part of the Atlantic Tradewind Ocean-Atmosphere Mesoscale Interaction Campaign (ATOMIC). *Earth Syst. Sci. Data*, *13*(4), 1759–1790. https://doi.org/10.5194/essd-13-1759-2021

Rauber, R. M., Stevens, B., Ochs, H. T., Knight, C., Albrecht, B. A., Blyth, A. M., Fairall, C. W., Jensen, J. B., Lasher-Trapp, S. G., Mayol-Bracero, O. L., Vali, G., Anderson, J. R., Baker, B. A., Bandy, A. R., Burnet, E., Brenguier, J.-L., Brewer, W. A., Brown, P. R. A., Chuang, R., … Zuidema, P. (2007). Rain in Shallow Cumulus Over the Ocean: The RICO Campaign. *Bulletin of the American Meteorological Society*, *88*(12), 1912–1928. https://doi.org/10.1175/BAMS-88-12-1912

Reid, J. S., Hobbs, P. v, Ferek, R. J., Blake, D. R., Martins, J. V., Dunlap, M. R., & Liousse, C. (1998). Physical, chemical, and optical properties of regional hazes dominated by smoke in Brazil. *Journal of Geophysical Research: Atmospheres*, *103*(D24), 32059–32080. https://doi.org/https://doi.org/10.1029/98JD00458

Reid, J. S., Koppmann, R., Eck, T. F., & Eleuterio, D. P. (2005). A review of biomass burning emissions part II: intensive physical properties of biomass burning particles. *Atmospheric Chemistry and Physics*, *5*(3), 799–825. https://doi.org/10.5194/acp-5-799-2005

Remoundaki, E., Bourliva, A., Kokkalis, P., Mamouri, R. E., Papayannis, A., Grigoratos, T., Samara, C., & Tsezos, M. (2011). PM10 composition during an intense Saharan dust transport event over Athens (Greece). *Science of The Total Environment*, *409*(20), 4361–4372. https://doi.org/https://doi.org/10.1016/j.scitotenv.2011.06.026

Roberts, G. C., Artaxo, P., Zhou, J., Swietlicki, E., & Andreae, M. O. (2002). Sensitivity of CCN spectra on chemical and physical properties of aerosol: A case study from the Amazon Basin. *Journal of Geophysical Research: Atmospheres*, *107*(D20), LBA 37-1-LBA 37-18. https://doi.org/https://doi.org/10.1029/2001JD000583

Roberts, G. C., & Nenes, A. (2005). A Continuous-Flow Streamwise Thermal-Gradient CCN Chamber for Atmospheric Measurements. *Aerosol Science and Technology*, *39*(3), 206–221. https://doi.org/10.1080/027868290913988

Roberts, G., Wooster, M. J., & Lagoudakis, E. (2009). Annual and diurnal african biomass burning temporal dynamics. *Biogeosciences*, *6*(5), 849–866. https://doi.org/10.5194/bg-6-849-2009

Rogers, C. F., Hudson, J. G., Zielinska, B., Tanner, R. L., Hallett, J., & Watson, J. G. (1991). *Cloud condensation nuclei from biomass burning*. Massachusetts Inst of Tech Press. http://inis.iaea.org/search/search.aspx?orig_q=RN:23066783

Rolph, G., Stein, A., & Stunder, B. (2017). Real-time Environmental Applications and Display sYstem: READY. *Environmental Modelling & Software*, *95*, 210–228. https://doi.org/https://doi.org/10.1016/j.envsoft.2017.06.025

Rose, D., Gunthe, S. S., Mikhailov, E., Frank, G. P., Dusek, U., Andreae, M. O., & Pöschl, U. (2008). Calibration and measurement uncertainties of a continuous-flow cloud condensation nuclei counter (DMT-CCNC): CCN activation of ammonium sulfate and sodium chloride aerosol particles in theory and experiment. *Atmospheric Chemistry and Physics*, *8*(5), 1153–1179. https://doi.org/10.5194/acp-8-1153-2008

Rosenfeld, D., Rudich, Y., & Lahav, R. (2001). Desert dust suppressing precipitation: A possible desertification feedback loop. *Proceedings of the National Academy of Sciences*, *98*(11), 5975 LP – 5980. https://doi.org/10.1073/pnas.101122798

Russell, L. M., Hawkins, L. N., Frossard, A. A., Quinn, P. K., & Bates, T. S. (2010). Carbohydrate-like composition of submicron atmospheric particles and their production from ocean bubble bursting. *Proceedings of the National Academy of Sciences*, *107*(15), 6652 LP – 6657. https://doi.org/10.1073/pnas.0908905107

Sareen, N., Schwier, A. N., Lathem, T. L., Nenes, A., & McNeill, V. F. (2013). Surfactants from the gas phase may promote cloud droplet formation. *Proceedings of the National Academy of Sciences*, *110*(8), 2723–2728. https://doi.org/10.1073/pnas.1204838110

Savoie, D. L., Arimoto, R., Keene, W. C., Prospero, J. M., Duce, R. A., & Galloway, J. N. (2002). Marine biogenic and anthropogenic contributions to non-sea-salt sulfate in the marine boundary layer over the North Atlantic Ocean. *Journal of Geophysical Research: Atmospheres*, *107*(D18), AAC 3-1-AAC 3-21. https://doi.org/https://doi.org/10.1029/2001JD000970

Schill, G. P., Froyd, K. D., Bian, H., Kupc, A., Williamson, C., Brock, C. A., Ray, E., Hornbrook, R. S., Hills, A. J., Apel, E. C., Chin, M., Colarco, P. R., & Murphy, D. M. (2020). Widespread biomass burning smoke throughout the remote troposphere. *Nature Geoscience*, *13*(6), 422–427. https://doi.org/10.1038/s41561-020-0586-1

Shen, H., Peters, T. M., Casuccio, G. S., Lersch, T. L., West, R. R., Kumar, A., Kumar, N., & Ault, A. P. (2016). Elevated Concentrations of Lead in Particulate Matter on the Neighborhood-Scale in Delhi, India As Determined by Single Particle Analysis. *Environmental Science & Technology*, *50*(10), 4961–4970. https://doi.org/10.1021/acs.est.5b06202

Sobanska, S., Coeur, C., Maenhaut, W., & Adams, F. (2003). SEM-EDX Characterisation of Tropospheric Aerosols in the Negev Desert (Israel). *Journal of Atmospheric Chemistry*, *44*(3), 299–322. https://doi.org/10.1023/A:1022969302107

Sobanska, S., Falgayrac, G., Rimetz-Planchon, J., Perdrix, E., Brémard, C., & Barbillat, J. (2014). Resolving the internal structure of individual atmospheric aerosol particle by the combination of Atomic Force Microscopy, ESEM–EDX, Raman and ToF–SIMS imaging. *Microchemical Journal*, *114*, 89–98. https://doi.org/https://doi.org/10.1016/j.microc.2013.12.007

Sorooshian, A., Corral, A. F., Braun, R. A., Cairns, B., Crosbie, E., Ferrare, R., Hair, J., Kleb, M. M., Hossein Mardi, A., Maring, H., McComiskey, A., Moore, R., Painemal, D., Scarino, A. J., Schlosser, J., Shingler, T., Shook, M., Wang, H., Zeng, X., … Zuidema, P. (2020). Atmospheric Research Over the Western North Atlantic Ocean Region and North American East Coast: A Review of Past Work and Challenges Ahead. *Journal of Geophysical Research: Atmospheres*, *125*(6), e2019JD031626. https://doi.org/https://doi.org/10.1029/2019JD031626

Spracklen, D. v, Carslaw, K. S., Pöschl, U., Rap, A., & Forster, P. M. (2011). Global cloud condensation nuclei influenced by carbonaceous combustion aerosol. *Atmospheric Chemistry and Physics*, *11*(17), 9067–9087. https://doi.org/10.5194/acp-11-9067-2011

Stein, A. F., Draxler, R. R., Rolph, G. D., Stunder, B. J. B., Cohen, M. D., & Ngan, F. (2015). NOAA's HYSPLIT Atmospheric Transport and Dispersion Modeling System. *Bulletin of the American Meteorological Society*, *96*(12), 2059–2077. https://doi.org/10.1175/BAMS-D-14-00110.1

Stevens, B., Bony, S., Farrell, D., Ament, F., Blyth, A., Fairall, C., Karstensen, J., Quinn, P. K., Speich, S., Acquistapace, C., Aemisegger, F., Albright, A. L., Bellenger, H., Bodenschatz, E., Caesar, K.-A., Chewitt-Lucas, R., de Boer, G., Delanoë, J., Denby, L., … Zöger, M. (2021). EUREC4A. *Earth Syst. Sci. Data*, *13*(8), 4067–4119. https://doi.org/10.5194/essd-13-4067-2021

Stevens, B., Farrell, D., Hirsch, L., Jansen, F., Nuijens, L., Serikov, I., Brügmann, B., Forde, M., Linne, H., Lonitz, K., & Prospero, J. M. (2016). The Barbados Cloud Observatory: Anchoring Investigations of Clouds and Circulation on the Edge of the ITCZ. *Bulletin of the American Meteorological Society*, *97*(5), 787–801. https://doi.org/10.1175/BAMS-D-14-00247.1

Talbot, R. W., Andreae, M. O., Berresheim, H., Artaxo, P., Garstang, M., Harriss, R. C., Beecher, K. M., & Li, S. M. (1990). Aerosol chemistry during the wet season in central Amazonia: The influence of long-range transport. *Journal of Geophysical Research: Atmospheres*, *95*(D10), 16955–16969. https://doi.org/https://doi.org/10.1029/JD095iD10p16955

Tomlin, J. M., Jankowski, K. A., Veghte, D. P., China, S., Wang, P., Fraund, M., Weis, J., Zheng, G., Wang, Y., Rivera-Adorno, F., Raveh-Rubin, S., Knopf, D. A., Wang, J., Gilles, M. K., Moffet, R. C., & Laskin, A. (2021). Impact of dry intrusion events on the composition and mixing state of particles during the winter Aerosol and Cloud Experiment in the Eastern North Atlantic (ACE-ENA). *Atmospheric Chemistry and Physics*, *21*(24), 18123–18146. https://doi.org/10.5194/acp-21-18123-2021

Tsamalis, C., Chédin, A., Pelon, J., & Capelle, V. (2013). The seasonal vertical distribution of the Saharan Air Layer and its modulation by the wind. *Atmos. Chem. Phys.*, *13*(22), 11235–11257. https://doi.org/10.5194/acp-13-11235-2013

Twohy, C. H., Kreidenweis, S. M., Eidhammer, T., Browell, E. v., Heymsfield, A. J., Bansemer, A. R., Anderson, B. E., Chen, G., Ismail, S., DeMott, P. J., & van den Heever, S. C. (2009). Saharan dust particles nucleate droplets in eastern Atlantic clouds. *Geophysical Research Letters*. https://doi.org/10.1029/2008GL035846

Twomey, S. (1974). Pollution and the planetary albedo. *Atmospheric Environment (1967)*, *8*(12), 1251–1256. https://doi.org/https://doi.org/10.1016/0004-6981(74)90004-3

Twomey, S. (1977). The Influence of Pollution on the Shortwave Albedo of Clouds. *Journal of Atmospheric Sciences*, *34*(7), 1149–1152. https://doi.org/10.1175/1520-0469(1977)034<1149:TIOPOT>2.0.CO;2

Wang, Q., Saturno, J., Chi, X., Walter, D., Lavric, J. v, Moran-Zuloaga, D., Ditas, F., Pöhlker, C., Brito, J., Carbone, S., Artaxo, P., & Andreae, M. O. (2016). Modeling investigation of light-absorbing aerosols in the Amazon Basin during the wet season. *Atmospheric Chemistry and Physics*, *16*(22), 14775–14794. https://doi.org/10.5194/acp-16-14775-2016

Wex, H., Dieckmann, K., Roberts, G. C., Conrath, T., Izaguirre, M. A., Hartmann, S., Herenz, P., Schäfer, M., Ditas, F., Schmeissner, T., Henning, S., Wehner, B., Siebert, H., & Stratmann, F. (2016). Aerosol arriving on the Caribbean island of Barbados: physical properties and origin. *Atmos. Chem. Phys.*, *16*(22), 14107–14130. https://doi.org/10.5194/acp-16-14107-2016

Wu, H., Taylor, J. W., Langridge, J. M., Yu, C., Allan, J. D., Szpek, K., Cotterell, M. I., Williams, P. I., Flynn, M., Barker, P., Fox, C., Allen, G., Lee, J., & Coe, H. (2021). Rapid transformation of ambient absorbing aerosols from West African biomass burning. *Atmospheric Chemistry and Physics*, *21*(12), 9417–9440. https://doi.org/10.5194/acp-21-9417-2021

Yu, H., Tan, Q., Chin, M., Remer, L. A., Kahn, R. A., Bian, H., Kim, D., Zhang, Z., Yuan, T., Omar, A. H., Winker, D. M., Levy, R., Kalashnikova, O., Crepeau, L., Capelle, V., & Chedin, A. (2019). Estimates of African Dust Deposition Along the Trans-Atlantic Transit Using the Decade-long Record of Aerosol Measurements from CALIOP, MODIS, MISR, and IASI. *Journal of Geophysical Research. Atmospheres : JGR*, *124*(14), 7975–7996. https://doi.org/10.1029/2019JD030574

Zauscher, M. D., Wang, Y., Moore, M. J. K., Gaston, C. J., & Prather, K. A. (2013). Air Quality Impact and Physicochemical Aging of Biomass Burning Aerosols during the 2007 San Diego Wildfires. *Environmental Science & Technology*, *47*(14), 7633–7643. https://doi.org/10.1021/es4004137

Zhang, R., Khalizov, A. F., Pagels, J., Zhang, D., Xue, H., & McMurry, P. H. (2008). Variability in morphology, hygroscopicity, and optical properties of soot aerosols during atmospheric processing. *Proceedings of the National Academy of Sciences*, *105*(30), 10291–10296. https://doi.org/10.1073/pnas.0804860105

Zuidema, P., Alvarez, C., Kramer, S. J., Custals, L., Izaguirre, M., Sealy, P., Prospero, J. M., & Blades, E. (2019). Is Summer African Dust Arriving Earlier to Barbados? The Updated Long-Term In Situ Dust Mass Concentration Time Series from Ragged Point, Barbados, and Miami, Florida. *Bulletin of the American Meteorological Society*, *100*(10), 1981–1986. https://doi.org/10.1175/BAMS-D-18-0083.1

Zuidema, P., Sedlacek III, A. J., Flynn, C., Springston, S., Delgadillo, R., Zhang, J., Aiken, A. C., Koontz, A., & Muradyan, P. (2018). The Ascension Island Boundary Layer in the Remote Southeast Atlantic is Often Smoky. *Geophysical Research Letters*, *45*(9), 4456–4465. https://doi.org/https://doi.org/10.1002/2017GL076926

Zuidema, P., Xue, H., & Feingold, G. (2008). Shortwave Radiative Impacts from Aerosol Effects on Marine Shallow Cumuli. *Journal of the Atmospheric Sciences*, *65*(6), 1979–1990. https://doi.org/10.1175/2007JAS2447.1

Supporting Information: African Smoke Acts as Cloud Condensation Nuclei in the Wintertime Tropical North Atlantic Boundary Layer over Barbados

Haley M. Royer[1], Mira L.-Pöhlker[2,3,4*] Ovid Krüger[2], Edmund Blades[5,6], Peter Sealy[5], Nurun Nahar Lata[7], Zezhen Cheng[7], Swarup China[7], Andrew P. Ault[8], Patricia K. Quinn[9], Paquita Zuidema[1], Christopher Pöhlker[2], Ulrich Pöschl[2], Meinrat Andreae[2,10,11], and Cassandra J. Gaston[1*]

[1]Department of Atmospheric Sciences, Rosenstiel School of Marine,~~ and~~ Atmospheric, and Earth Science, University of Miami, Miami, FL 33149

[2]Department of Multiphase Chemistry, Max Planck Institute for Chemistry, Mainz, Germany 55128

[3]Leipzig Institute for Meteorology, Leipzig University, Leipzig, Germany

[4]Experimental Aerosol and Cloud Microphysics Department, Leibniz Institute for Tropospheric Research, Leipzig, Germany

[5]Barbados Atmospheric Chemistry Observatory, Ragged Point, Barbados

[6]Queen Elizabeth Hospital Barbados, Bridgetown, Barbados

[7]Environmental Molecular Sciences Laboratory, Pacific Northwest National Laboratory, Richland, WA

[8]Department of Chemistry, University of Michigan, Ann Arbor, MI 48109

[9]Pacific Marine Environmental Laboratory, National Oceanic and Atmospheric Administration, Seattle, WA 98115

[10]Department of Geology and Geophysics, King Saud University, Riyadh, Saudi Arabia

[11]Scripps Institution of Oceanography, University of California San Diego, La Jolla, California, USA

Formatted: Line spacing: single

Formatted: Not Strikethrough

*Corresponding Authors:

Mira L. Pöhlker: Email: poehlker@tropos.de, Phone: +49 6131 305 7020

Cassandra J. Gaston: Email: cgaston@ ~~rsmas.~~miami.edu, Phone: (305)-421-4979

Details on the K-Means Clustering Algorithm and the Particle Identification Process

Formatted: Line spacing: Double

Data from CCSEM/EDX analysis were imported into MatLab 2019b (MathWorks, Inc.) as a matrix of relative elemental abundances for each single particle in a sample. The data were then analyzed using k-means clustering in which groups of similar particles (clusters) are generated based on the presence and intensity of elemental peaks in the spectra of individual particles. To utilize k-means clustering, the user sets the number of clusters that the algorithm will generate. The k-means clustering algorithm will then generate clusters based on similarities between the elemental composition of individual particles. Cluster numbers were chosen based on the optimal trade-off between error minimization and chemical composition representativeness of the dataset after running the algorithm with different cluster numbers for the same sample.

To determine the identity of particles in a cluster, 4 plots are utilized that provide detailed information on size, shape and chemistry. These plots include a particle size distribution plot, a circularity plot, a weight matrix detailing the relative % of each of the 16 elements of interest in the particles, and a digital color stack plot that provides information on the distribution of elements throughout the particles in the cluster. An absolute intensity of 1% for elemental abundance presented in the weight matrix was used as a threshold value to consider an element present in a cluster. Upon identification of particle types, number fractions for each particle type can be calculated by summing together similar particle types and dividing by the total number of particles analyzed. These number fractions were generated for Fig. 4, 5, and 7. For figures 4 and 7, specific particle type number fractions were determined by dividing the number of specific particles in a particle type by the total number of particles analyzed in one day of sampling. For

Fig. 5, number fractions were generated by dividing the number of particles of one particle type by the total number of particles in each size range plotted in the figure.

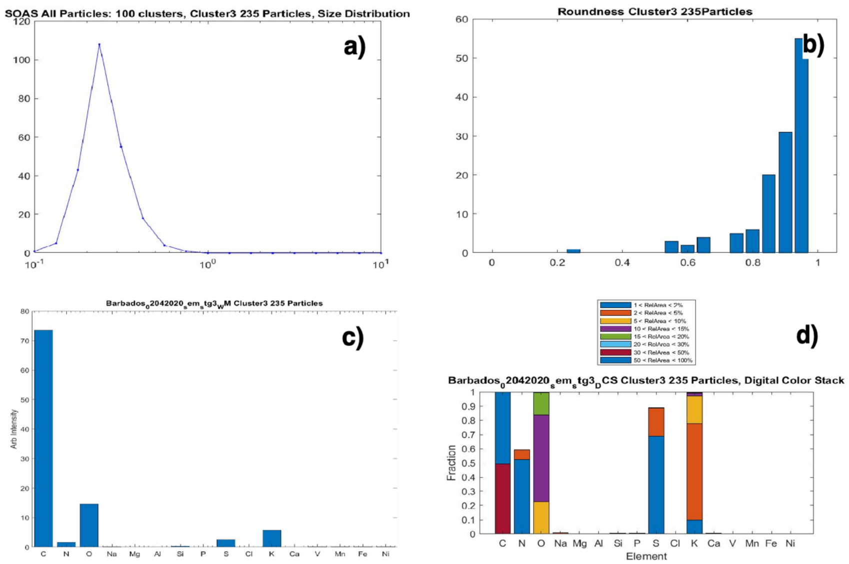

Figure S1 – Plots generated from the k-means clustering algorithm used for particle identification including a) a particle size distribution plot, b) a circularity plot, c) a weight matrix presenting relative abundance of elements in the cluster, and d) a digital color stack plot. The digital color stack plot describes the fraction of particles that contained each element of interest (height of bar) as well as the fraction of particles in the cluster in which an element made up a specific range of relative areas (size of colored bars and color of bar).

Formatted: Line spacing: Double, Keep with next

Formatted: Font: Times, 12 pt, Not Italic, Font color: Text 1

Temporal Chemistry Plots for the Supermicron Particle Loading

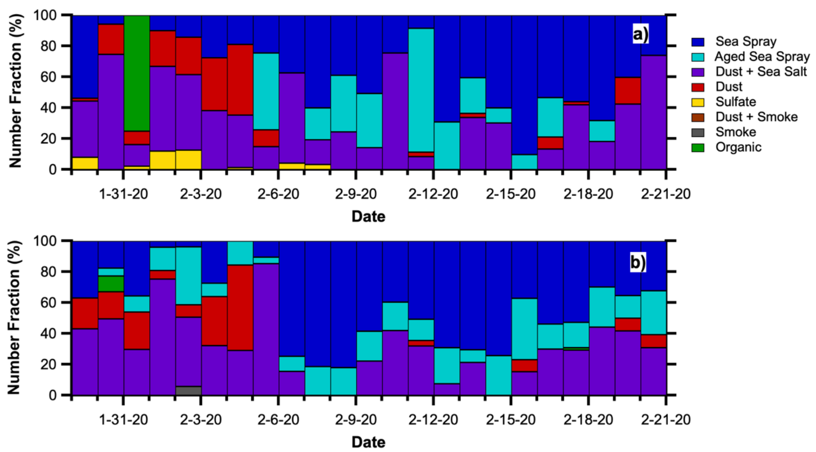

Figure S2 - Temporal evolution of particle type number fractions for a) stage 1 and b) stage 2 of the multistage particle sampler analyzed using CCSEM/EDX.

Formatted: Font: Times, 12 pt

Formatted: Line spacing: Multiple 1.08 li

Formatted: Font: (Default) Times, 12 pt, Bold, Font color: Auto

Formatted: Line spacing: Double, Keep with next

Formatted: Font: Times, 12 pt, Not Italic, Font color: Text 1

~~1.~~ African Fire Distribution and Intensity During EUREC4A/ATOMIC ~~Map~~

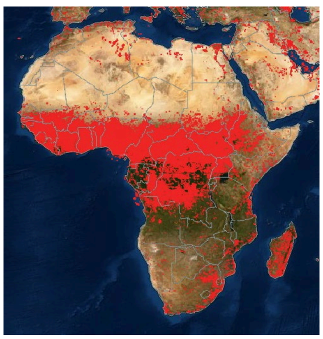

Figure S3~~1~~ – Active fires (red shading) present between January 29th through February 20th of 2020 plotted using NASA’s Fire Information for Resource Management System (FIRMS) model. Red shading is produced using NOAA’s Visible Infrared Imaging Radiometer Suite (VIIRS NOAA-20), which shows active fire detections and thermal anomalies.

Formatted: Normal, No bullets or numbering

Formatted: Font: Times, Bold

Formatted: Line spacing: Double

Formatted: Line spacing: Double

Formatted: Line spacing: Double

I. **CO Column Density Measurements during EUREC⁴A/ATOMIC**

Formatted: Font: (Default) Times New Roman, 12 pt, Bold, Font color: Text 1

Formatted: Normal, Line spacing: Double, No bullets or numbering

Formatted: Line spacing: Double

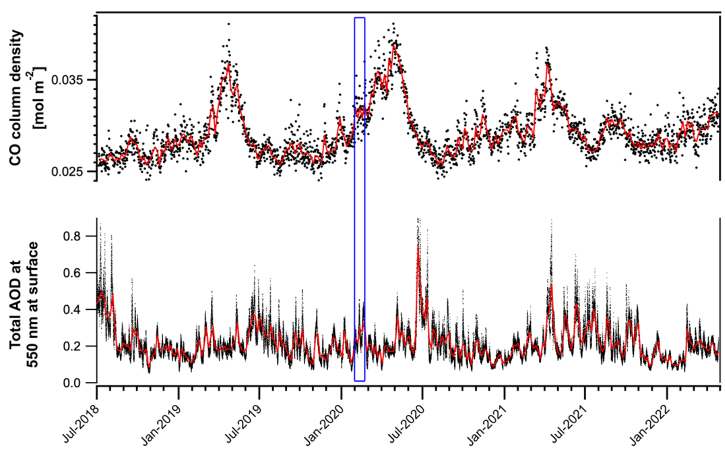

Figure S42 – Vertically integrated cCarbon monoxide (CO) column density measurements and total aerosol optical depth collected from July 2018 through January 2022 at BACO. CO measurements were obtained from the Sentinel-5P Near Real-Time Carbon Monoxide dataset. AOD data were obtained from the Copernicus Atmosphere Monitoring Service (CAMS). O. Region outlined in blue box indicates time period for EUREC⁴A/ATOMIC campaigns.

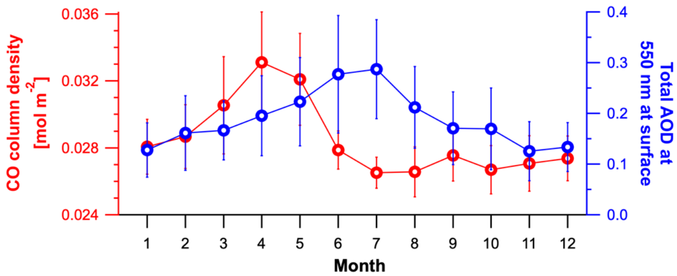

Figure S5~~3~~ – Monthly averages for vertically integrated carbon monoxide (CO; a proxy for smoke) column density and~~,~~ aerosol optical depth~~, and aerosol optical thickness~~ collected at Barbados from 2018 – 2022, 2016 – 2022, and 1983 – 2022, respectively.~~ ~~ CO measurements were obtained from the Sentinel-5P Near Real-Time Carbon Monoxide dataset. AOD data were obtained from the Copernicus Atmosphere Monitoring Service (CAMS).

Formatted: Font: Bold

Formatted: Line spacing: Double

III. Size-Resolved Chemistry of CAT Event 2 and 3 During EUREC^{4}A/ATOMIC

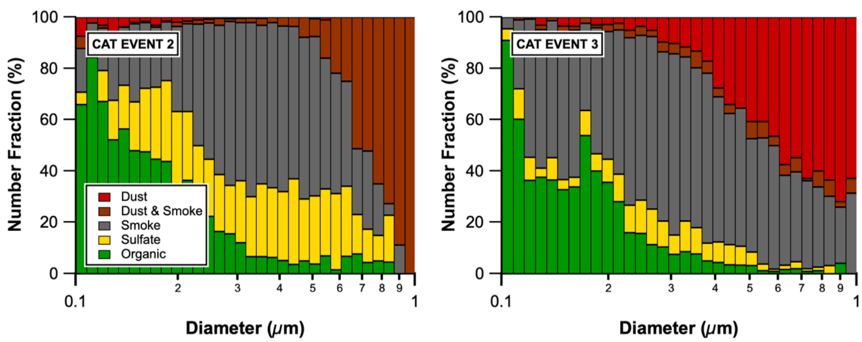

Figure S64 – Number fractions of 6 main submicron particle types plotted as a fraction of aerodynamic diameter (Da). CAT Event 2 and 3 includes size-resolved chemical data from the 2nd (2/10/2020 0:00 – 2/12/2020 6:00 GMT) and 3rd (2/15/2020 12:00 – 2/20/2020 18:00 GMT) period in which dust and wildfire smoke were observed over Barbados, respectively. Particle counts in bins for CAT Event 2 range from 9 to 476 particles, with an average bin size of 253 particles. Particle counts in bins for CAT Event 3 range from 22 to 792 particles, with an average bin size of 266 particles.

Sampling Period	Day/Time	Average Diameter (μm)					
		Organic	Sulfate	Smoke	Aged Sea Spray	Dust	Dust + Smoke
Clean Marine	2020/1/29 0:00 – 2020/1/29 12:00	---	0.40+0.15	0.26+0.11	---	0.70+0.29	---
CAT Event 1	2020/1/29 18:00 – 2020/2/6 6:00	0.18+0.08	0.26+0.15	0.27+0.13	---	0.56+0.29	0.48+0.34
Clean Marine	2020/2/6 12:00 – 2020/2/9 18:00	0.20+0.10	0.28+0.12	0.39+0.23	0.26+0.08	0.69+0.24	0.74+0.61
CAT Event 2	2020/2/10 0:00 – 2020/2/12 6:00	0.19+0.08	0.28+0.12	0.30+0.12	---	0.18+0.07	---
Clean Marine	2020/2/12 12:00 – 2020/2/15 6:00	0.23+0.08	0.30+0.15	0.22+0.08	---	---	0.62+0.35
CAT Event 3	2020/2/15 12:00 – 2020/2/20 – 18:00	0.19+0.08	0.27+0.11	0.29+0.16	---	0.56+0.30	0.39+0.29

Table S1 - Average particle diameters for each particle type determined for each sampling condition observed during the field campaign.

Formatted: Font: (Default) Times New Roman, 12 pt, Bold, Font color: Text 1

Formatted: Normal, Line spacing: Double, No bullets or numbering

Formatted: Font: (Default) Times New Roman, 12 pt, Bold, Font color: Text 1

Formatted: Line spacing: Double

Formatted: Font: (Default) Times New Roman, 12 pt, Font color: Text 1

Formatted: Centered, Line spacing: single

Formatted Table

Formatted: Keep with next

Formatted: Font: Times, 12 pt, Not Italic, Font color: Text 1

Formatted: Font: Times, 12 pt, Not Italic, Font color: Text 1

Mean and Median values of Total Smoke Particle Count Analyzed with CCSEM/EDX

Sampling Period	**Day/Time**	**Mean Smoke Particles Analyzed (#)**	**Median Smoke Particles Analyzed (#)**
CAT Event 1	2020/1/29 18:00 – 2020/2/6 6:00	1985	1011
CAT Event 2	2020/2/10 0:00 – 2020/2/12 6:00	1094	848
CAT Event 3	2020/2/15 12:00 – 2020/2/20 – 18:00	948	500

Table S2 - Mean and median values of total smoke particles analyzed using CCSEM/EDX~~.~~

~~Values are calculated~~ for each CAT Event observed throughout the field campaign.

Comparison of Smoke # Fraction and CCN counts for each day of EUREC4A/ATOMIC

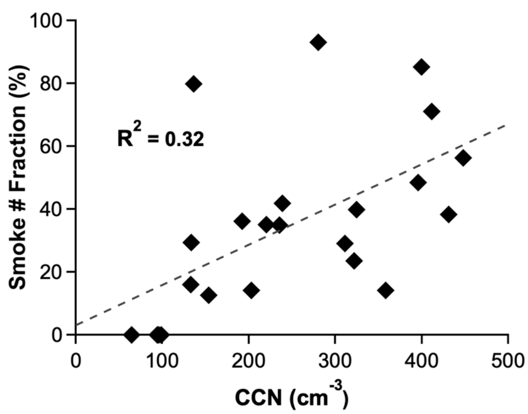

Figure S7 - Correlation plot comparing smoke particle number# fraction from samples collected on stage 3 of the particle impactor and analyzed with CCSEM/EDX to CCN counts averaged for each day of the sampling period.

Formatted: Font: Times, 12 pt, Bold

Formatted: Font: Times, 12 pt, Bold, Not Italic

Formatted: Line spacing: single

Formatted: Font: +Body (Calibri), 11 pt, Italic, Font color: Auto

Formatted: Normal, Line spacing: single

Formatted: Font: Times, 12 pt, Bold

Formatted: Font: (Default) Times, Bold, Italic, Font color: Auto

Formatted: Line spacing: Double, Keep with next

Formatted: Font: Times, 12 pt, Not Italic, Font color: Text 1

Formatted: Caption, Line spacing: Double

Formatted: Font: Times, 12 pt, Not Italic, Font color: Text 1

Formatted: Font: Times, 12 pt, Not Italic, Font color: Text 1

Formatted: Font: (Default) Times, Italic

Formatted: Normal